**University of Bath**

**Alternative formats**
If you require this document in an alternative format, please contact:
openaccess@bath.ac.uk

## Accepted Article

**Title:** Biomass-derived carbons for sodium-ion batteries and sodium-ion capacitors

**Authors:** Libo Deng, Jianhui Zhu, James Roscow, Sundaram Chandrasekaran, Peixin Zhang, Tingshu He, Kuo Wang, and Licong Huang

A Journal of

ChemPubSoc
Europe

## WILEY-VCH

www.chemsuschem.org

# Biomass-derived carbons for sodium-ion batteries and sodium-ion capacitors

Jianhui Zhu[a,b], James Roscow[c], Sundaram Chandrasekaran[b], Libo Deng[b*],

Peixin Zhang[a,b*], Tingshu He[a], Kuo Wang[b] and Licong Huang[b]

[a] College of Materials Science and Engineering, Xi'an University of Architecture and Technology, Xi'an, Shannxi 710055, PR China

[b] College of Chemistry and Environmental Engineering, Shenzhen University, Shenzhen 518060, China

[c] Materials and Structures Centre, Department of Mechanical Engineering, University of Bath, Claverton Down, Bath, BA2 7AY, UK

## Abstract

In the past decade, the rapid development of portable electronic devices, electric vehicles and electrical devices has stimulated extensive interests in fundamental research and commercialization of electrochemical energy storage systems. Biomass-derived carbon has garnered significant research attention as an efficient, inexpensive and eco-friendly active material for energy storage systems. Therefore, high-performance carbonaceous materials, derived from renewable sources, have been utilized as electrode materials in sodium-ion batteries

* Corresponding authors: Denglb@szu.edu.cn; pxzhang@szu.edu.cn

and sodium-ion capacitors. In this review, we summarize the charge storage mechanism and utilization of biomass-derived carbon for sodium storage in batteries and capacitors. In particular, the structure-performance relationship of biomass-derived carbon for sodium storage in the form of batteries and capacitors is discussed. Despite the fact that further research is required to optimize the process and application of biomass-derived carbon in energy storage devices, the current review demonstrates the potential of carbonaceous materials for next-generation sodium-involved energy storage applications.

**Keywords:** Biomass; sodium-ion battery; sodium-ion capacitor; electrochemistry

## 1. Introduction

Renewable and cleaner energy resources, such as wind, solar and nuclear, are being extensively researched due to the increasing energy demand, depleting fossil fuel reserves and environmental concerns. However, the successful realization of renewable energy technology requires the development of efficient, cost-effective and large-scale energy storage systems (ESSs).[1,2]

Li-ion batteries (LIBs), currently the most widely employed energy storage devices, were commercialized by Sony in the 1990s and attained ubiquitous status in modern life.[3] However, the large-scale development

2

of LIBs is hindered by the cost of lithium (Li) metal due to limited resources. Only 20 ppm Li exists in Earth's crust, leading to the extremely high cost of Li-containing salts and active materials.[4] Sodium (Na), on the other hand, is the fourth most abundant metal element (2.74%) in Earth crust and exhibits similar chemical properties to Li (**Fig. 1**), arousing extensive research interest as a possible replacement of Li metal in rechargeable batteries.[4-7] Sodium-ion batteries (SIBs) were first studied in the 1970s, but the rapid development and successful commercialization of LIBs diverted the research focus from SIBs.[1,8-11] Despite the similar energy storage mechanism of SIBs and LIBs, some differences still exist between them. For example, the difference in ionic radii of $Na^+$ ions (1.02 Å) and $Li^+$ ions (0.76 Å) hinders the common electrodes in LIBs to be used in SIBs.[12] Moreover, the higher molar mass and standard electrode potential of Na (23 g $mol^{-1}$ and -2.71 V *vs.* SHE) compared to Li (6.9 g $mol^{-1}$ and -3.02 V *vs.* SHE) lead to a lower energy density.[1] However, the charge storage capacity is mainly determined by the structural features of the electrode materials and both Na and Li contribute only a small part of the electrode weight. Therefore, the difference in the energy density of LIBs and SIBs has negligible consequences.[6] Furthermore, aluminum (Al) can be utilized as an anode current collector instead of copper (Cu) in SIBs because, unlike Li, Na does not react with Al. This represents a significant potential cost

3

reduction if SIBs could be widely utilized. However, low power density and poor cyclic performance raise serious concerns on the development and commercialization of SIBs.
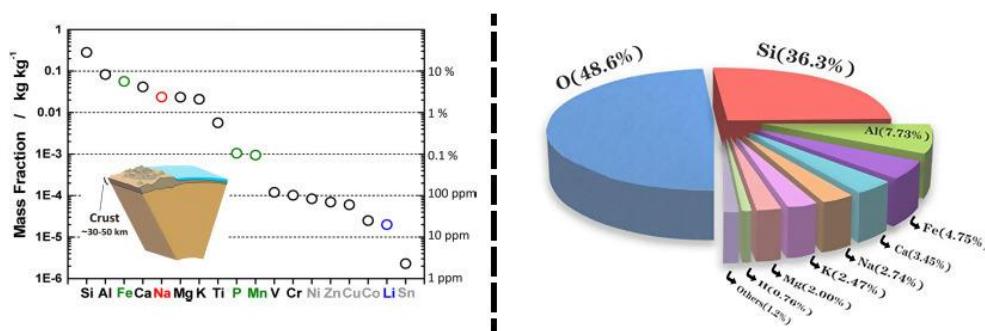


**Figure 1.** The distribution of different elements in Earth's crust. Reproduced (adapted) with permission from Ref. 4. Copyright 2014 American Chemical Society

Electrochemical capacitors are promising alternatives or complementary technology to secondary batteries due to their high power densities and superior cyclic performance. Charge storage in an electrochemical capacitor is limited to the electrode surface, leading to lower charge storage capacity and inferior energy density. On the other hand, hybrid-ion capacitors combine the advantages of battery-type and electric double layer capacitive (EDLC) materials, which might exhibit high energy density, high power density and ultra-long lifetime simultaneously. Li-ion capacitors (LICs) are the most prominent hybrid-ion capacitors, possessing relative high energy density, power

4

density and cyclic life. However, similar to LIBs, the high cost and scarcity of Li-metal hinder the large-scale utilization of LICs. As such, sodium-ion capacitors (SICs) are potential candidates for large-scale energy storage applications due to the cost and the abundance of Na. The development of high-performance SICs is limited by the slow kinetics of battery-type anode and low capacitance of activated carbon (AC) cathode in organic electrolytes, where the former leads to unfavorable rate capability and inferior cyclic stability, and the later leads to low energy density.[13,14] Therefore, the electrochemical properties of both cathode and anode should be optimized to make them suitable for commercial SICs.

Different carbonaceous materials have been extensively studied as electrode materials for sodium ion batteries and capacitors due to their accessibility, non-toxicity and high chemical stability.[15-19] However, the carbon materials still exhibit several disadvantages, including high manufacturing cost, complex synthesis processes and environmental pollution. Recently, biomass, derived from green plants, land- and water-based vegetation and organic wastes, has been employed as an environment-friendly precursor for carbonaceous materials.[20] It is worth noting that biomass is the third-largest energy resource after coal and oil and dominated the global energy consumption until the mid-19th century before being overtaken by fossil fuels. Biomass-derived carbon is a

5

pyrolytic product of biomass, which offers a green and effective way of biomass utilization. The various applications, morphology and performance of different biomass-derived carbons are shown in **Table 1**. Typically, biomass-derived carbon displays a specific morphology, such as fibers[21] or nanosheets[22], which is highly desirable for energy storage devices, as shown in **Fig. 2**. Significantly, biomass-derived carbon possesses advantages to obtain high-performance structures,[23] such as the naturally porous features, hierarchical and/or fiber structures of biomass that can be remained in the pyrolyzed product. These features enable effective penetration of the electrolyte into the structure and shorten the ion diffusion route. Moreover, elements such as nitrogen (N), boron (B) etc., exist in natural biomass, which remain as heteroatoms after processing, enhancing the electrical conductivity and absorption, thus improving the electrochemical performance of biomass-derived carbons.[23- 25 ] Furthermore, the utilization of biomass for carbon production is a cost-effective and eco-friendly approach because it enables recyclability of different waste materials, such as banana peel[26], macadamia shells[27], cellulose[28,29] and lignin[30,31,32].

Table 1 Application of biomass-derived carbon in energy storage

| Precursor | Morphology | Application | Capacity | Current density $(mA\ g^{-1})$ | ICE | Ref. |
|-----------|-----------|-------------|----------|--------------------------------|-----|------|
| Ramie fibers | Rod-like | LIB | 432 mAh g$^{-1}$ | 100 | 57% | [33] |
| Coconut oil | Nanoparticles | LIB | 742 mAh g$^{-1}$ | 100 | 55% | [34] |

6

| Wheat straw | Nanosheets | LIB | 502 mAh g$^{-1}$ | 37.2(0.1C) | 62.9% | [35] |
|---|---|---|---|---|---|---|
| Prosopis juliflora | Tube-like | LIC | 108 mAh g$^{-1}$ | 50 | - | [36] |
| Egg white | Microporous | LIC | 184 F g$^{-1}$ | 400 | - | [37] |
| Apricot shell | Porous | SIB | 400 mAh g$^{-1}$ | 25 | 79% | [72] |
| Oak leaf | Porous | SIB | 358.6 mAh g$^{-1}$ | 10 | 74.8% | [38] |
| Lotus stem | Hierarchical structure | SIB | 351 mAh g$^{-1}$ | 40 | 70% | [39] |
| Fe-carrageenan | Fibers | SIB | 317 mAh g$^{-1}$ | 1000 | 68.9% | [94] |
| Cherry petals | Nanosheets | SIB | 310.2 mAh g$^{-1}$ | 20 | 67.3% | [40] |
| Cotton stalk | Porous | SIC | 160.5 F g$^{-1}$ | 200 | - | [133] |
| Corn silk | nanosheets | SIC | 126 F g$^{-1}$ | 300 | - | [41] |
| Bamboo | Porous | Supercapacitor | 318 F g$^{-1}$ | 200 | - | [42] |
| Bean dregs | Porous | Supercapacitor | 482 F g$^{-1}$ | 1000 | - | [43] |
| Soybean Pods | Porous | Supercapacitor | 321.1 F g$^{-1}$ | 1000 | - | [44] |
| eggplant | Flakes | Supercapacitor | 327 F g$^{-1}$ | 1000 | | [45] |
| tofu | Porous | Supercapacitor | 315 F g$^{-1}$ | 500 | | [46] |
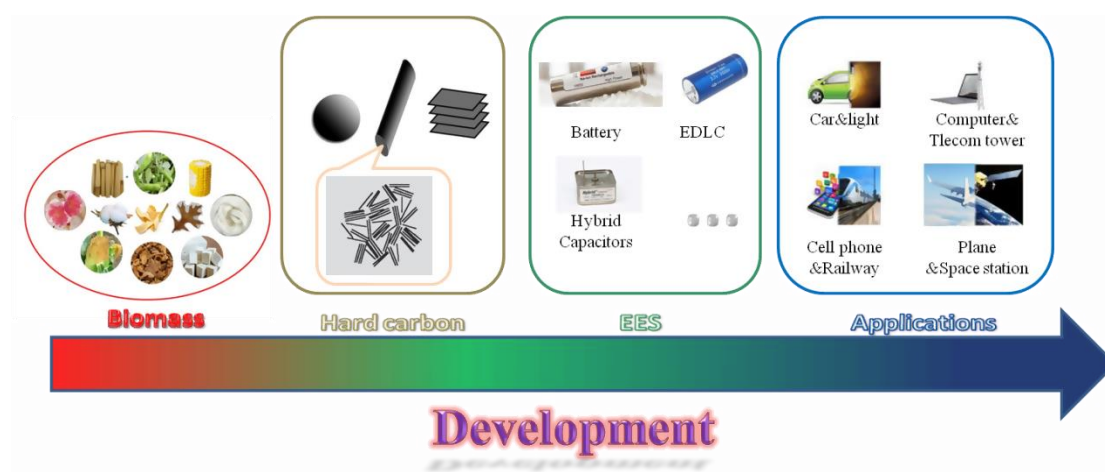


**Figure 2.** The utilization and properties of biomass-derived carbon in different applications.

The present review summarizes the utilization of biomass-derived carbon in SIBs and SICs. First, the principle and mechanism of

7

carbonaceous materials for energy storage is discussed, before detailing recent research into biomass-derived carbon for SIBs and SIC. The current understanding of the structure-performance relationship of biomass-derived carbon is discussed in terms of the electrode material in SIBs and SICs. Finally, we discuss the challenges remained for application of biomass-derived carbon in SIBs and SICs, and provide an outlook on future directions for the development of biomass-derived carbon for energy storage applications.

## 2. Biomass-derived carbon for SIBs

## 2.1 Principle and mechanism

A battery consists of three basic components: an anode, a cathode and an electrolyte. In the case of SIBs, Na ions shuttle between the anode and cathode compartments during the charge/discharge process. The choice of anode material significantly influences the performance of SIBs because it can limit the rate of electrochemical reactions. One should note that, unlike cathode materials, a limited number of anode materials are available for SIBs due to dendrite formation and the relatively low melting point of Na.

Different forms of carbon-based materials, including graphite-based carbon, graphene, soft and hard carbons, have been investigated as anode materials in SIBs.[47] Theoretically, it has been confirmed that Na ions can be easily intercalated into carbonaceous materials with an interlayer

8

distance higher than 0.37 nm[48], as shown in **Fig. 3a**. As the interlayer distance between graphite sheets is only 0.335 nm, natural graphite only possesses a low theoretical charge storage capacity. Similarly, Na ions cannot penetrate into voids of soft carbon due to its interlayer distance (<0.35 nm) and random orientation of layers, and as such Na ions tend to absorb on the surface and defect sites of soft carbon.[49] In the case of graphene, the absorption characteristics are improved by high surface area, which yields more sites for Na ions adsorption. The galvanostatic charge-discharge profiles of graphite-based carbon, soft carbon and graphene are shown in **Fig. 3b**, where a monotonically decreasing capacity is observed with the interesting potential. Moreover, different types of carbons display different reversible capacities and initial coulomb efficiency (ICE). In summary, the charge storage mechanism of these three types of carbonaceous materials for SIBs is that Na ions only adsorbed on electrochemically active surface and defect sites.

9
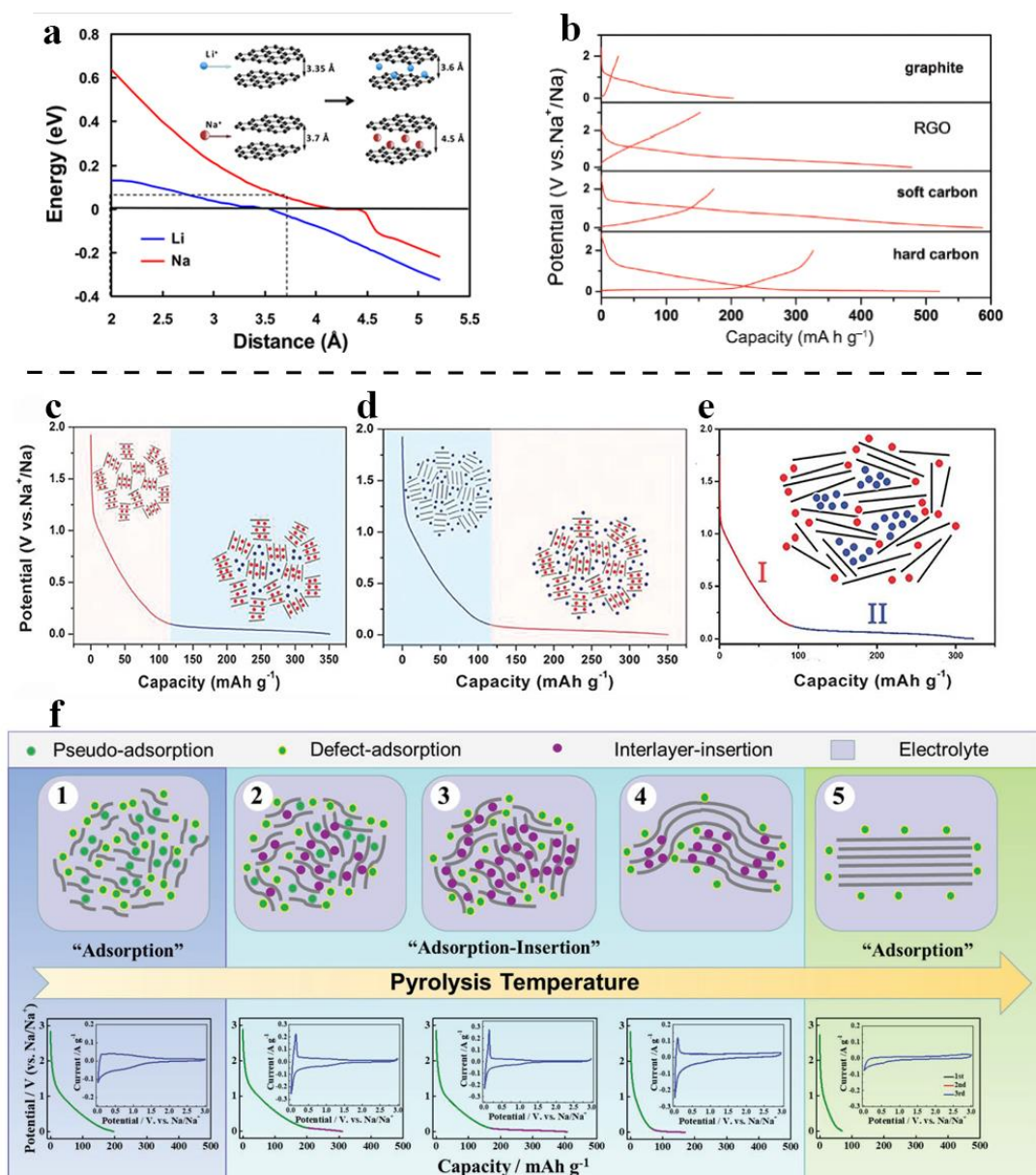
**Figure 3.** (a) Theoretical energy cost for Na (red curve) and Li (blue curve) ions insertion into carbon as a function of carbon interlayer distance. The inset illustrates the mechanism of Na- and Li-ions insertion into carbon. Reproduced (adapted) with permission from Ref. 48. Copyright 2012 American Chemical Society; (b) the 1st cycle galvanostatic charge-discharge profiles of different carbonaceous materials in NaClO4/EC+DEC electrolyte; Reproduced (adapted) with permission from Ref. 50. Copyright 2017 Science China Press; (c) schematic illustration of the intercalation-adsorption mechanism for Na

10

storage in hard carbon; (d) schematic illustration of the adsorption-intercalation mechanism of Na storage in hard carbon; Reproduced (adapted) with permission from Ref. 52. Copyright 2017, Wiley-VCH. and (e) schematic illustration of Na storage mechanism in cotton-derived hard carbon microtubes. Reproduced (adapted) with permission from Ref. 53. Copyright 2016, Wiley-VCH. (f) Schematic illustration of the evolution of the microstructure, sodium storage mechanism and behavior with the pyrolysis temperature of HCs. Reproduced with permission from Ref. 55 Copyright 2019, Wiley-VCH.

Compared with graphite-based carbon, soft carbon and graphene, the charge storage mechanism of hard carbon is more complicated. Two clear regions, usually labelled as the sloping region and plateau region, can be readily observed from the voltage-capacity curve of hard carbon, as shown in **Fig. 3b**.[50] These regions indicate the presence of different charge storage mechanisms, as proposed by various research groups.[48,51,53] An insertion-absorption mechanism was first proposed by Stevens and Dahn in 2001[51], as shown in **Fig. 3c**. The results of *in-situ* X-ray scattering demonstrated that the interlayer distance of adjacent carbon layers of dehydrated glucose changes significantly in the sloping region. Moreover, by using *in-situ* small-angle X-ray scattering, they confirmed that the electron density contrast within the nanopores decreased with $Na^+$ insertion and increased with $Na^+$ desertion during the low-potential plateau region. From these results, they concluded that the

11

sloping potential profiles in the high voltage region corresponded to the intercalation of Na ions, whereas Na ions were inserted into nanopores along the low-voltage plateau. In 2012, Cao et al. [48] reported on the sodium storage behavior of hollow carbon nanowires and proposed an absorption-insertion mechanism. They suggested that Na ions were adsorbed on the surface of hollow carbon nanowires during the high-potential sloping region and inserted into voids during the low-potential plateau region, as shown in **Fig. 3d**. Later, the proposed mechanism was confirmed by using a combination of *in-situ* X-ray diffraction mapping, *ex-situ* nuclear magnetic resonance (NMR), electron paramagnetic resonance (EPR) and electrochemical characterization techniques.[52] Specifically, at the beginning of Na insertion, $Na^+$ adsorb on defects of hard carbon which contributes to sloping voltage profiles. Flat low voltage plateaus are formed after intercalation of Na ions into interlayers with enough space to form $NaC_x$. Furthermore, Hu et al. synthesized hard carbon microtubes and reported that the *d*-spacing remained the same before and after discharging, as shown in **Fig. 3e**, which cannot be explained by the above-mentioned charge storage mechanisms.[53] Therefore, it is of utmost importance to establish a new adsorption-filling mechanism, where Na ions are expected to absorb at the defect sites, edges and the surface of graphitized nanodomains in the sloping region and fill the nanovoids in the plateau region. Besides, a

12

three-step charge storage mechanism has been proposed by Bommier et al.,[54] where Na ions adsorb on defect sites in the high potential regions and get inserted into the hard carbon as well as adsorb at the surface of the pores in the low potential regions.

One of the reasons for various charge storage mechanisms proposed so far is the inconsistence of the structure of various hard carbons prepared by different research groups. To unify these storagre mechanisms, Sun et al.[55] established an extended "Adsorption-Insertion" model and revealed the relationship between charge storage mechanism and structure of hard carbon. They obtained hard carbon with different microstructures by carbonizing fallen ginkgo leaves at different temperatures ranging from 600 ℃ to 2500 ℃. The development of the microstructure as well as the charge storage mechanism and performance are shown in Fig. 3f. At low temperatures, the hard carbon possesses a highly disordered structure with a large interlayer distance ( > 0.4 nm). The large interlayer distance is enough for Na ions to undergo "pseudo-adsorption" behavior similar to sodium storage behavior of "defect adsorption" in this stage. It contributes to slope capacity together with other "defects" (pores, edges, heteroatoms, etc) above 0.1 V. No phase transformation or structural change occurrs during the charge/discharge process and thus HCs in this stage usually have an excellent cycle and rate performance. As the carbonization temperature

13

increases, the highly disordered structures rearrange and is transformed into microcrystallite. At this stage, the interlayer distance decreases to 0.36-0.40 nm, leading to a more difficult migration of Na ions. However, this interlayer distance is large enough for "interlayer insertion" of Na$^+$ and the charge storage mechanism change from "pseudo-adsorption" into "interlayer insertion". In addition, some conventional defects still exists in hard carbon and provide some sloping capacity *via* "defect adsorption". Although the hard carbon at this stage possesses high capacity, the cycle stability and rate performance is worse than the highly disordered carbon. When the carbonized temperatures further increase, the hard carbon is converted into a graphite-like state with a low interlayer distance (<0.36 nm) and few residual defects and void. At this stage, the interlayer distance is too small for Na$^+$ to insert into interlayer such that only a small sloping region resulting from the residual defects and void can be observed, resulting in a capacity that is too low to utilized in a battery. Such a extended "adsorption-insertion" model unravlled the relationship between the microstructure of hard carbon and its charge storage mechanism. It provides new insight into the design and development of advanced hard carbon anode materials for SIBs.

## 2.2 Classification of biomass-derived carbons

Raw biomass has to be converted into a useful carbon form for application in ESSs. The conductive networks and interconnected

14

channels, which facilitate the movement of ions and electrons, are formed *via* carbonization. In general, biomass-derived carbons for sodium storage are utilized in the form of nanocarbon with a nanoscale size (<100 nm) in at least one dimension (micro-scale powders with nanopores for electrochemical application can be considered as aggregates of nanoparticles), and thus can be classified into four types according to their morphology. Zero dimensional (0D) refers to a material with nanoscale size in all dimensions (such as nanospheres); one dimensional (1D) refers to nanofibers, nanorods, and nanotubes, etc which have nanoscale sizes in two directions; two dimensional (2D, i.e. sheets or flakes) and three dimensional (3D, i.e. aggregates or assembles of nanomaterials).

### 2.2.1 0D carbons

0D carbons have been extensively utilized as anode materials in SIBs due to their mechanical robustness and ability to restrict volumetric changes. In 2014, Hu et al.[17] developed monodispersed hard carbon spherules *via* the hydrothermal method which is a relatively simple method for biomass conversion that has gained increasing research attention. The monodispersed hard carbon spherules have been carbonized at different temperatures and the influence of carbonization temperature on microstructure and electrochemical performance has been systematically investigated. The resulting hard carbon exhibited perfect

15

spherules shape with a smooth surface and uniform particle size (~ 1 μm), which was independent of the carbonization temperature (**Fig. 4a**). During the hydrothermal process, the dewatered sugar (semi-fluid) was isolated out from water and formed an aqueous emulsion under high temperature and high pressure.[56] The excessive amount of dewatered sugar led to the formation of tiny particles, consisting of nuclei-oligomers within micelle, and finally formed carbon nanospheres after the complete consumption of sugar. The XRD pattern and Raman spectra, presented in **Fig. 4b-d**, indicate that the degree of the disorder increased with the increasing carbonization temperature, which seems counter-intuitive. It has been reported that the growth and orientation of graphite domains increase with the increasing annealing temperature.[57] However, such a dependence has not been explained yet, and thus requires further investigation. Furthermore, an interesting phenomenon was observed in galvanostatic discharge-charge profiles (**Fig. 4e-f**). It is clear that hard carbon microspherules carbonized at 1600 ℃ (HCS1600) displayed a poor rate capability. When HCS1600 electrode was discharged (Na insertion) at a constant current rate of 0.1 C and charged (Na extraction) at different rates, an ultrahigh reversible charge capacity of 270 mAh $g^{-1}$ is achived at a charging rate of 20 C. It indicated that the insertion step limits the rate performance of hard carbon.
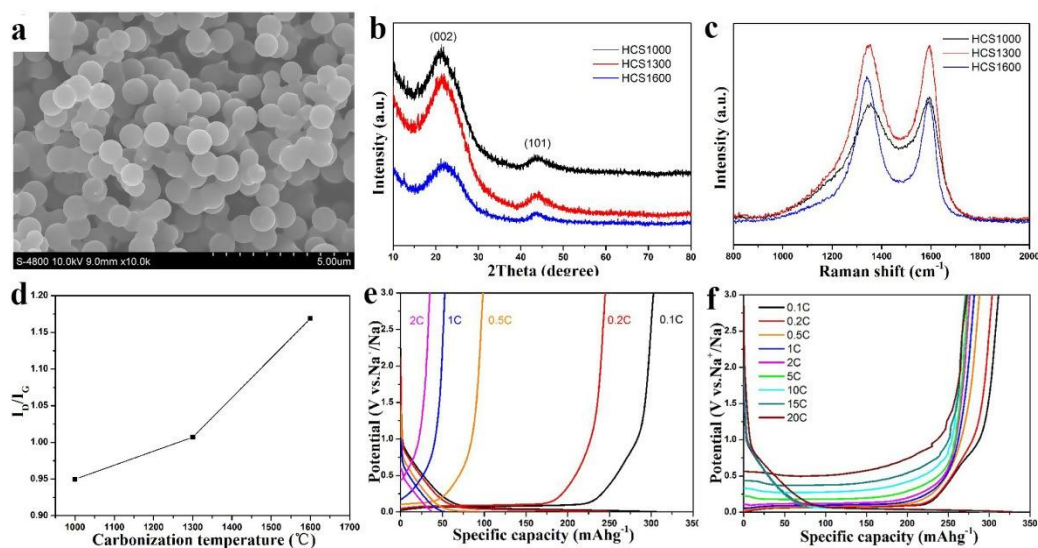
**Figure 4.** Characterization of HCS carbonized at different temperatures: (a) SEM image; (b) XRD patterns; (c) Raman spectra; (d) the relationship between $I_D/I_G$ and carbonization temperature; (e) rate performance of HCS1600; and (f) HCS1600 electrodes, discharged at the same current rate of 0.1 C. Reproduced (adapted) with permission from Ref. 17. Copyright 2014, The Royal Society of Chemistry.

## 2.2.2 1D carbons

1D materials offer distinct advantages for SIBs by enabling interconnected electron transport channels between the active material and current collector. Moreover, the composites of 1D carbons exhibit large surface areas and appropriate pore size distributions that enables optimal contact area between the electrode and electrolyte, which can shorten the ionic diffusion.

One should note that morphology of the precursor has a significant effect on the resulting microstructure of the biomass-derived carbon. Li et

17

al.[53] carbonized cotton under argon (Ar) to prepar hard carbon microtubes (HCTs). A fiber shape with hollow structure was obtained after high-temperature carbonization, which could facilitate the electrolyte transport and reduce the diffusion distance for Na ions. Galvanostatic intermittent titration technique (GITT) measurements revealed that the coefficient of Na ions diffusion was different in sloping and plateau regions due to different binding energies for Na-carbon interaction. This indicates that the capacity from the sloping region is available for high-power SIBs, which can also be utilized to develop high-energy SIBs by combining the contribution from the low-voltage plateau. The full-cell SIB consisting of HCTs anode that carbonized at 1300 ℃ and a $Na_{0.9}[Cu_{0.22}Fe_{0.30}Mn_{0.48}]O_2$ cathode, exhibited a high energy density of 207 Wh $kg^{-1}$, excellent rate capability with a specific capacity of 220 mAh $g^{-1}$ at a high current rate of 1 C, and superior cyclic stability. Moreover, Yang et al.[58] reported an extension on bacterial cellulose, special natural cellulose synthesized by certain bacteria, i.e., A*cetobacter xylinum*, to produce nitrogen (N)-doped carbon as an anode material for SIBs by using the hydrothermal method, as shown in **Fig. 5a.** The as-prepared carbon was utilized as a free-standing anode and delivered a relatively stable capacity of 154 mAh $g^{-1}$ after 1500 cycles at a current density of 400 mA $g^{-1}$.

18
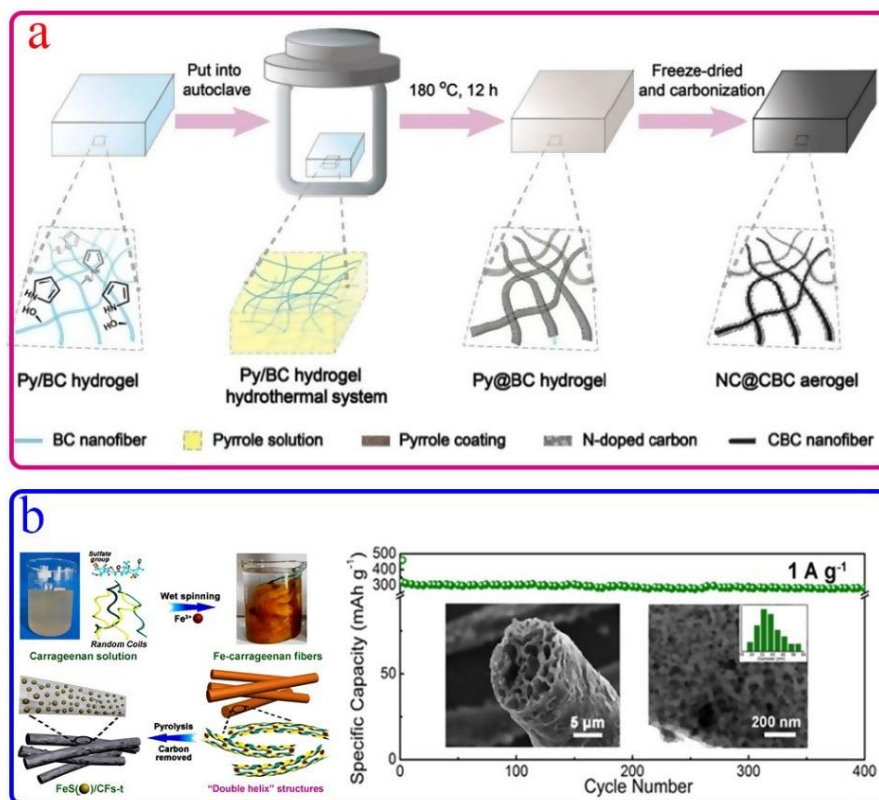
**Figure 5.** (a) A schematic illustration of the synthesis of N-doped carbon. Reproduced from Ref. 58 with permission from the Centre National de la Recherche Scientifique (CNRS) and The Royal Society of Chemistry. (b) FeS/CFs. Reproduced (adapted) with permission from Ref.94. Copyright 2018 American Chemical Society

Fiber-like materials are frequently synthesized by using spinning, a method that uses a spinneret to form multiple continuous polymer filaments or monofilaments that involves the rapid and continuous condensing of a liquid to a solid-state with a limited size in two directions.[59] Li et al.[94] used Fe-carrageenan, a kind of Fe-containing biomass, to synthesized nanocomposites (FeS/CFs) combining iron sulfide (FeS) nanoparticles (NPs, 25-45 nm) with carbon microfibers

19

(CF, diameter: ~10-15 μm) by using wet-spinning before carbonization to fabricate FeS/carbon anode for SIBs. As shown in **Fig. 5b**, the ι-carrageenan solution was extruded from a spinneret into a coagulating bath containing $Fe^{3+}$ ethanol solution to form Fe-carrageenan fibers. In this process, the random coil carrageenan macromolecules gelated with $Fe^{3+}$ ions, which contributed to form a double-helix structure, accelerated the aggregation of different double helices and formed junction zones that ensure the long-range cross-linking of biomass microfibers. Fe-carrageenan fibers were then transformed into FeS/CFs after pyrolysis under an inert atmosphere. Finally, the FeS/CFs was treated by a post-treatment at 600 ℃ under $CO_2$ for 1-2 h. The FeS/CFs calcined at 600 ℃ for 1 h (FeS/CFs-1) had an optimal carbon content of 20.9 wt.% and a high reversible capacity of 317 mAh $g^{-1}$. Moreover, excellent rate performance and cyclic stability (283 mAh $g^{-1}$ after 400 cycles) were achieved. On the other hand, FeS/CFs calcined at 600 ℃ for 2 h (FeS/CFs-2) exhibited severe volumetric changes during the charge/discharge process, causing serious agglomeration and pulverization of carbon microfibers, and leading to inferior cyclic performance.

### 2.2.3 2D carbons

2D carbon nanostructures have been regarded as a potential structure for SIBs and have attracted great attention.[60-63] It exhibits high specific

20

surface area, continuous electron conduction path and the ability to sustain volumetric changes during charge/discharge process.[64] Yang et al.[65] fabricated N-doped carbon nanosheets by using okara as a carbon precursor, which contains protein, fat, fiber and a high N content (~9.89%). The carbonized okara was exfoliated to enhance the interlayer distance between carbon nanosheets and achieve a high specific surface area. When used as an anode material in a full SIB, N-doped carbon nanosheets delivered a high energy density of 146.1 Wh $kg^{-1}$, which is much higher than most of the SIBs reported previously.[66,67,68] Moreover, the stable discharge capacity of N-doped carbon nanosheets, with a mass loading of 1.40, 2.29, 4.56, 7.52 mg $cm^{-2}$, was found to be 247.5, 191.5, 141.7, and 121.7 mAh $g^{-1}$, respectively. These results show that N-doped carbon nanosheets meet the requirements for practical applications. Wang et al.[69] obtained a carbon nanosheet *via* pyrolyzing peanut skin. The SEM and TEM image showed that carbon nanosheets possess a thickness with tens of nanometers. $N_2$ adsorption/desorption isotherms indicated that the carbon nanosheets possesses a high specific surface area (2070 $m^2$ $g^{-1}$) as well as hierarchically micro-meso-macroporous. When employed as anode for SIBs, it delivered an ultrahigh reversible capacity of 461 mAh $g^{-1}$ at 0.1 A $g^{-1}$ and promising rate performance. This excellent performance is associated with the disordered structure for copious reversible binding of Na at the carbon defects.

21

## 2.2.4 3D carbons

3D porous structures are promising electrode materials for LIBs and SIBs[70,71,72] due to their high specific surface area and interconnected porous structure, providing a large number of electrolyte diffusion channels and reducing the diffusion distance of Na ions. Zhu et al.[72] synthesized porous hard carbons from waste apricot shells by carbonization. The as-prepared hard carbon retained the natural porous structure of the apricot shell, which facilitated the electrolyte pervasion and therefore led to superior electrochemical performance as an anode material in SIBs. The hard carbons carbonized at 1300 ℃ exhibited a specific capacity of 400 mAh g$^{-1}$ and an ICE of 79%. It is noted that H$_2$ reduction decreased the oxygen concentration and surface defects. In addition, the capacity plateau was not seen at a rate up to 4C, indicating that moderate defects are beneficial to the rapid diffusion of Na ions within the anode material. In addition, Hu et al.[73] obtained block-like hard carbon from a corn cob (HCC) *via* direct carbonization, as shown in **Fig. 6a**. The structure and morphology of HCC were investigated by using X-ray diffraction (XRD), Raman spectroscopy, high-resolution transmission electron microscopy (HRTEM) and selected area electron diffraction (SAED), as shown in **Fig. 6b-e**. The results indicated that HCC possesses a turbostratic structure, a typical feature of hard carbon which has a graphite-like layered structure but no stacking between the

22

bent layers.[74] Moreover, a large number of nanovoids (i.e. pores) within
the carbon were observed with increasing heat treatment temperature,
which was ascribed to a decreasing defect concentration, heteroatom
doping and the rearrangement of carbon atoms, leading to a higher
concentration of Na adsorption sites. Furthermore, HCC-derived carbon,
carbonized at 1300 ℃, exhibited a specific capacity of 275 mAh g$^{-1}$ and
excellent cyclic stability with a capacity retention of 97% after 1000
cycles. The highly disordered structure of HCC provided enough space
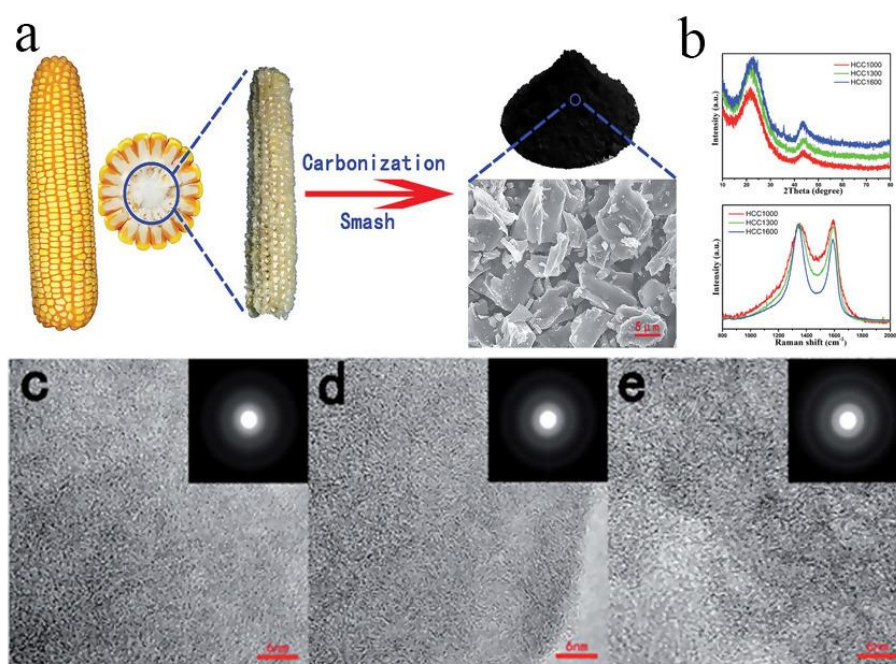for the transport and storage of Na ions, making it a promising anode for
SIBs.



**Figure 6.** (a) Schematic illustration of HCC synthesis from corncob by
carbonization and the corresponding SEM image; (b) XRD patterns and
Raman spectra of different HCCs; TEM images and SAED patterns of
HCCs obtained at (c)1000 ℃, (d) 1300 ℃ and (e) 1600 ℃. Reproduced
(adapted) with permission from Ref. 73. Copyright 2016, The Royal

23

Society of Chemistry.

## 2.3 Factors influence the performance for SIBs

## 2.3.1 Graphitization degree

A large number of studies have reported that higher graphitization degree and fewer defects in hard carbon can reduce the formation of "dead sodium", which significantly lowers the 1st cycle irreversible capacity loss. However, there are many randomly-distributed, disordered graphitic domains and pores in biomass-derived carbon.[75,76] In fact, it is difficult to convert biomass-derived carbon into graphite crystals by direct heating even at a high temperature of 3000℃.[75-79] Previous reports indicated that the high carbonization temperature and slow heating rate could modify the microstructure of carbon and, consequently, improve the electrochemical performance.[57,80] In this aspect, Zhao et al.[81] employed a low-temperature strategy to obtain hard carbon with graphite crystals by using egg-shell membranes and sucrose as carbon precursors. The precursors were sandwiched between two graphite blocks and sintered at 1300 ℃, as shown in **Fig. 7a**. A mixture of microspheres and graphite powders were sandwiched between two graphite blocks and calcinated to obtain microspheres with a higher degree of graphitization. The TEM image showd that the as-prepared carbon contains nanopores (**Fig. 7b-c**), graphite crystals and pseudo-graphitic structure with crystallite domains (<150 Å) along $c$-axis.[82] The biomass-derived carbon,

24

with graphite crystals, showed a high ICE of ~91% and a reversible capacity of 310 mAh g$^{-1}$. The adopted strategy exhibited a novel pathway to obtain high-quality hard carbon with high ICE. Furthermore, XRD and Raman spectroscopy results revealed that the presence of graphite crystals reduced the defect concentration and promoted a high level of ordering within pseudo-graphitic domains. Based on these results, a new growth mechanism was proposed. The carbon atoms from the precursor continuously accumulated around graphite nuclei, leading to long-range rearrangement of sp$^2$ carbon atoms. Moreover, the higher content of graphite crystals guarantees the interconnected pseudo-graphitic domains with a progressively more ordered structure and lower defect concentration, resulting in the formation of hard carbon with high crystallinity.
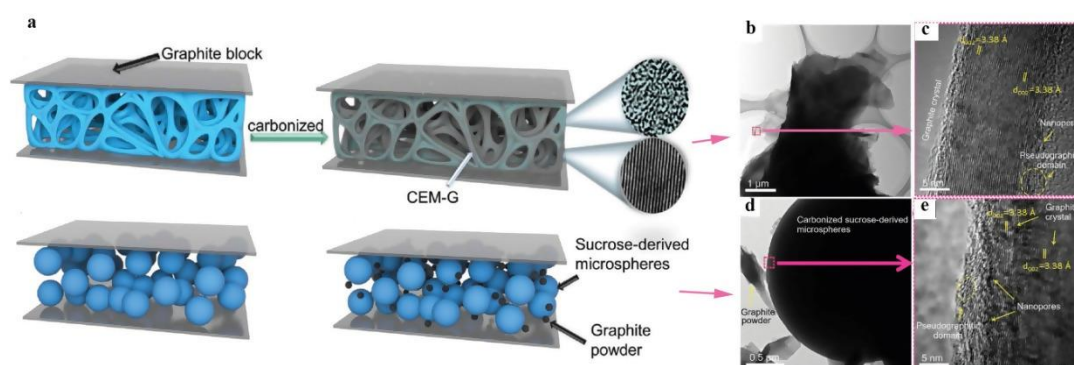


**Figure 7.** (a) Schematic illustration of the low-temperature growth of hard carbon materials with graphite crystals; (b) TEM and (c) HRTEM images of carbonized eggshell membranes with graphite crystals; (d) TEM and (e) HRTEM images of carbonized sucrose-derived microspheres with graphite crystals. Reproduced (adapted) with permission from Ref. 81 Copyright 2019, Wiley-VCH.

25

## 2.3.2 Morphology and specific surface area

Biomass-derived carbons synthesized *via* different routes possess different morphologies, and thus significant variation in electrochemical performance.[50,75,83] Numerous carbon morphologies, such as spherules, nanofibers and sheet-like structures, have been extensively studied for potential utilization in SIBs, as discussed in section 2.2. In general, the different morphologies of carbon materials result in a significant difference in electrochemical behavior.[84,85] Li et al.[70] prepared a range of carbons with different morphologies by using hydrothermal treatment of peanut skin. With the increase of sulfuric acid concentration (from 0 M to 6 M, products are denoted as CNSA-X, while X refers to the sulfuric acid concentration during the hydrothermal treatment) in the hydrothermal process, the morphology changed from large irregular particle with scattered pores to graphene-like nanosheet according to SEM and TEM inspection. Such a morphology evolution increased the performance significantly, leading to excellent cyclic and rate performance for CNSA-6 (i.e. with nanosheet morphology). The GCD curves of CNSA-6 showed a sloping shape, suggesting a reversible adsorption of $Na^+$ at the structural defect sites instead of insertion/exsertion of $Na^+$.

Specific surface area also influences the electrochemical

performance strongly. Li et al.[53] utilized cotton as a carbon precursor to obtain hard carbon with a uniform microtubular shape. The cotton roll was carbonized at 1000, 1300 and 1600 ℃ for 2 h under Ar, which were labeled as HCT1000, HCT1300, HCT1600, respectively. HCT1000 possessed a high specific surface area of 538 $m^2$ $g^{-1}$, whereas HCT1300 and HCT1600 exhibited lower specific surface areas, of 38 and 14 $m^2$ $g^{-1}$, respectively. The low specific surface area of HCT1300 and HCT1600 limited the formation of solid electrolyte interphase (SEI) and led to higher reversible capacities, as shown in **Fig. 8**. Moreover, the CV curves of HCT1000 indicated a potential adsorption-desorption mechanism of sodium storage, whereas HCT1300 and HCT1600 exhibited an absorption-filling Na storage mechanism. Furthermore, HCT1000 exhibited better rate performance than HCT1300 and HCT1600 due to the higher specific surface area, which increased the contact area between electrode and electrolyte and shortened the ionic diffusion distance. In addition, HCT1000 did not exhibit any significant capacity fading because the adsorption-desorption Na storage mechanism is similar to the capacitive storage.

27
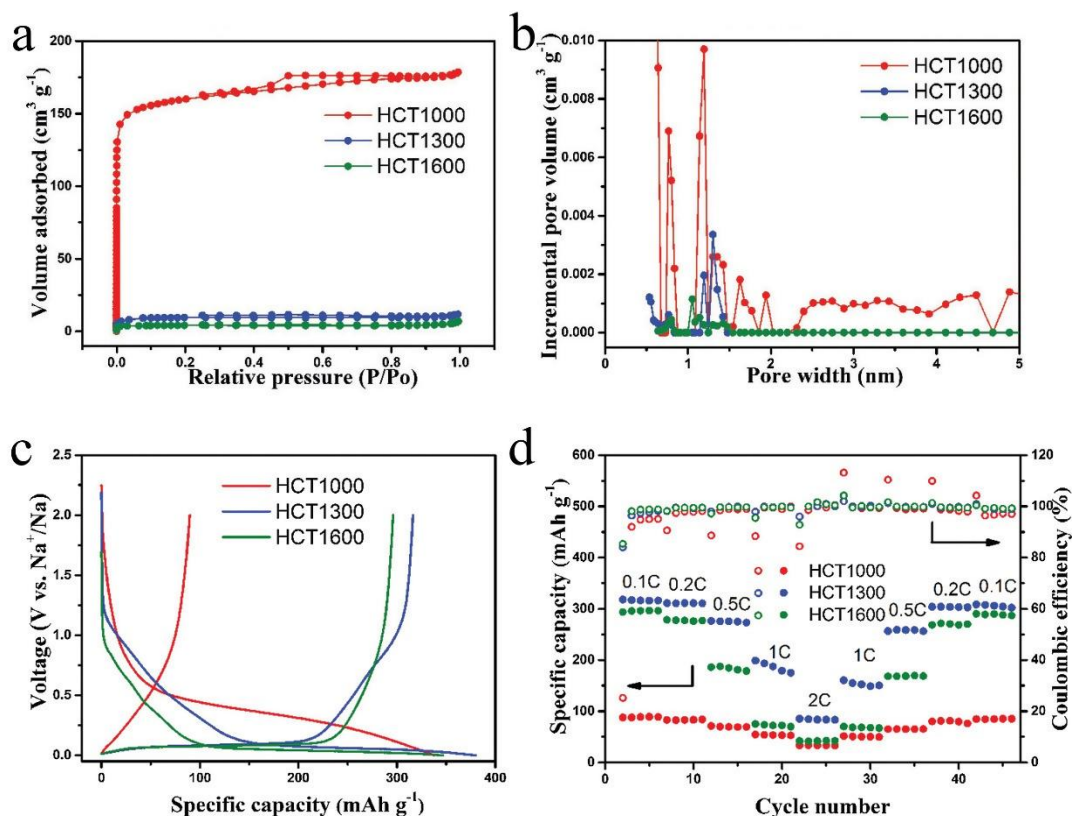
**Figure 8.** (a) $N_2$ adsorption-desorption isotherms of HCT and (b) the corresponding pore size distribution; (c) $1^{st}$ cycle galvanostatic discharge/charge profiles of HCT at a current rate of 0.1 C and (d) rate capability of HCT at different current rates (0.1 to 2 C). Reproduced (adapted) with permission from Ref. 53. Copyright 2016, Wiley-VCH.

### 2.3.3 Heteroatom doping

Heteroatom doping, which is considered as an effective way to enhance Na storage properties, has attracted significant research attention. In general, the electrochemical properties of carbon can be enhanced by heteroatom doping, which increases the interlayer spacing and decreases the barrier for the intercalation-deintercalation process.[86] Moreover, the presence of heteroatom in carbon structure improves the electrolyte

28

wettability and electrical conductivity.[87] Therefore, a large number of heteroatom-doped carbons have been developed as anode materials for SIBs.[75]

Carbonizing heteroatom-containing precursors is an effective method to introduce heteroatoms into the carbon framework. For instance, Ou et al.[88] reported a facile method to obtain porous carbon with a high specific surface area and optimal N-doping. The presence of N-dopant increased the electrical conductivity and enhanced the interlayer spacing of as-prepared carbon, leading to superior capacity of storage of Na ions. The X-ray photoelectron spectroscopy (XPS) technique was employed understand the bonding between N and C. The high-resolution N 1s spectrum can be deconvoluted into two peaks, located at 398.3 eV and 400.7 eV, which can be assigned to pyrrolic (N-5) and pyridinic (N-6) nitrogen atoms, respectively. These pyrrolic and pyridinic nitrogen atoms were distributed at the verge of the graphene layer and contributed to the adsorption of Na ions at the graphene surface, delivering a high reversible capacity of 261 mAh $g^{-1}$ at a current density of 100 mA $g^{-1}$. Moreover, an excellent rate performance was indicated by a reasonably high capacity of 104 mAh $g^{-1}$ at a high current density of 5 A $g^{-1}$. Finally, the as-prepared electrode offered a specific capacity of 220 mAh $g^{-1}$ after 100 cycles, indicating superior cyclic performance.

Alternatively, biomass-derived carbons can be annealed in the

29

presence of a heteroatom-containing compound to obtain doped carbon.[89]

For example, Wang et al.[16] synthesized a 3D dual-doped interconnected CF thin film by infiltrating $NH_4HB_4O_7 \cdot H_2O$ into a bacterial cellulose pellicle, followed by carbonization, as shown in **Fig. 9a**. XPS results confirmed the successful substitution of B and N atoms into the carbon framework. It is worth noting that the dual-doped carbonaceous materials combine the benefits of both elements and display superior performance than the single-atom doped carbon. Dual-doped carbonaceous materials presented discharge and charge capacities of 1888 mAh $g^{-1}$ and 691 mAh $g^{-1}$ at the 1st cycle, respectively, as well as excellent cyclic stability and superior rate performance (**Fig. 9b-e**). Furthermore, density functional theory (DFT) calculations suggested that the absorption energy of B-doped graphene (-1.79 eV) was around three times higher than pure graphene (-0.59 eV) and nine times higher than N-doped graphene (-0.22 eV). This study revealed that B-doping remarkably enhances the Na adsorption ability of graphene compared to N-doping. Moreover, the synergistic influence of B- and N-doping led to increased interlayer spacing, improved electrochemical activity and superior electrical conductivity. Therefore, dual doping is a promising strategy to produce high-performance carbonaceous materials for sodium-ion batteries.

30
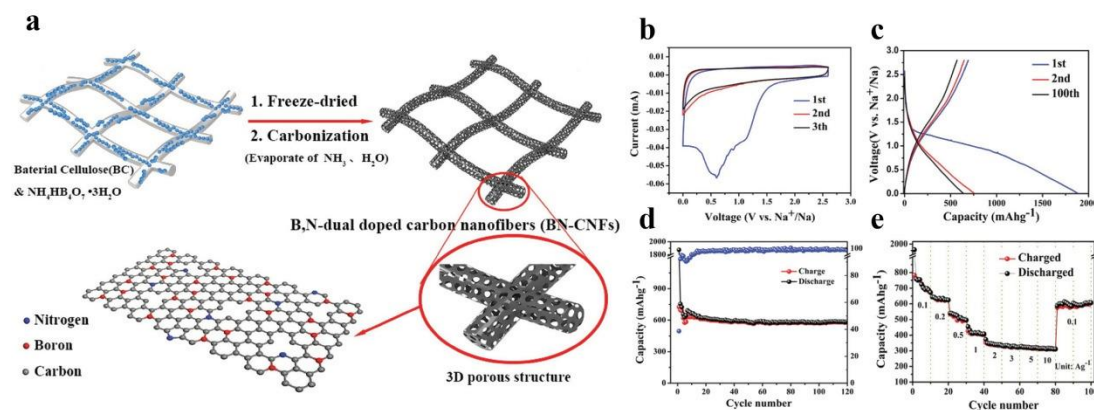
**Figure 9.** (a) Schematic illustration of the synthesis process of 3D dual-doped interconnected carbon fibers; (b) CV curves at a scan rate of 0.1 mV s$^{-1}$; (c) galvanostatic charge/discharge profiles at a current density of 100 mA g$^{-1}$; (d) cyclic performance at a current density of 100 mA g$^{-1}$; and (e) rate performance at different current densities, ranging from 0.1 to 10 A g$^{-1}$. Reproduced (adapted) with permission from Ref. 16. Copyright 2017, Wiley-VCH.

## 2.3.4 Hybrids of biomass-derived carbon and metallic compounds

Pristine and heteroatom-doped carbons have been extensively used as anode materials. However, their charge storage capacities are yet to be improved to meet the future demand. Recently, hybrids of biomass-derived carbon and metallic compounds, such as transition metal oxides, nitrides and sulfides, have been reported as superior anode materials for SIBs.[90, 91, 92] These carbon-based hybrids exhibit significantly improved charge storage capabilities, and excellent rate and cyclic performance due to the high capacity of metallic compounds, the conductive nature of carbon matrix and minimal volumetric changes

31

during charge/discharge process. The utilization of biomass-derived carbon is a novel route to synthesize carbon/metallic-compound hybrids for high-performance SIBs.

FeS is an excellent anode material for SIBs due to its high theoretical capacity of ~609 mAh g$^{-1}$.[93] Li et al.[94] utilized Fe-carrageenan biomass as a precursor to prepare 1D porous and FeS NPs/CF hybrids. The FeS/CFs-1 delivered a 1$^{st}$ cycle discharge and charge capacity of 460 and 317 mAh g$^{-1}$ at 1 A g$^{-1}$, respectively, corresponding to a Coulombic efficiency of 68.9%. Moreover, the charge capacity of 438, 376, 332, 303, 280 and 247 mAh g$^{-1}$ was achieved at the current density of 0.1, 0.2, 0.5, 1, 2 and 5 A g$^{-1}$, respectively. When the current density was restored to 0.1 A g$^{-1}$ after 60 cycles, the charge specific capacity was recovered to 431 mAh g$^{-1}$, which demonstrated the excellent rate capability of FeS/CFs-1. These results confirmed that the carbonaceous matrix maintained the structural stability of FeS NPs during the insertion/desertion process, which is crucial for stable cyclic performance. Dursun et al.[95] reported that 3D porous hybrids exhibit high capacity as anode materials in SIBs. They achieved simultaneous *in situ* coating of 5-nm-sized SnO$_2$ nanoparticles with bacterial cellulose, synthesizing the *Gluconoacetobacter xylinus strain* into the growth medium, to produce a SnO$_2$ nanoparticles-bacterial cellulose (SnO$_2$@PBC) hybrid that improved the cell performance. The 1$^{st}$ cycle

32

discharge capacity of $SnO_2/C$ composite was ~1100 mAh g$^{-1}$ and a reversible capacity of 400 mAh g$^{-1}$ had been attained after 400 cycles.

## 3. Biomass-derived carbon for SICs

## 3.1 Principle and mechanism

SICs, a kind of hybrid ion capacitors (HICs), offer battery-like energy density and supercapacitor-like power density and cyclic performance. As shown in **Fig. 10a**, SICs are usually composed of a non-faradaic material, a separator and a faradaic electrode material.[96-100] In a typical SIC, Na ions migrate to the anode during charging while electrolyte anions shift and adsorb to the cathode surface.[101] In the subsequent discharge process, they return back to the electrolyte. Both SIBs and SICs exhibit similar charge storage mechanism, which is based on faradic reactions of the active electrode materials.[102] However, the charge storage mechanism of SIBs is limited by the cation diffusion within the crystalline framework of the electrochemically active electrode material, whereas redox reactions occur only at the surface of the electrode material in SICs.

33
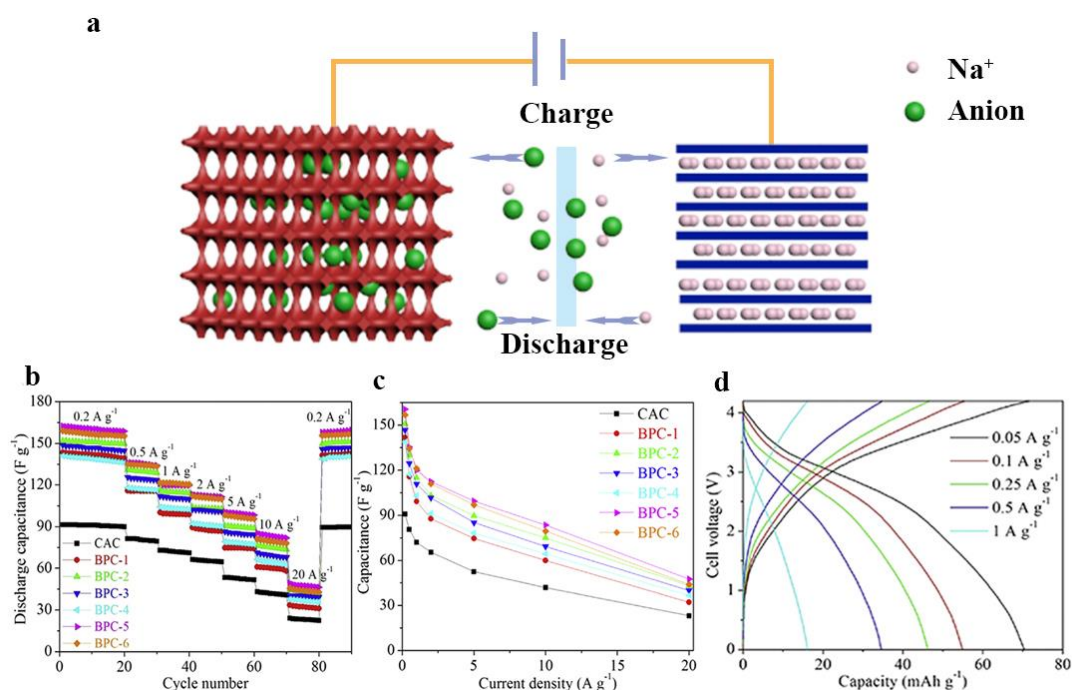
**Figure 10.** (a) The schematic illustration of Na-ion capacitors; (b) Rate performance and (c) capacitance of different biomass-derived carbons at various current densities, measured in a half-cell configuration in the voltage range of 2.0-4.2 V (*vs.* Na$^+$/Na); and (d) CV curves of SICs device at different current density. Reproduced (adapted) with permission from Ref. 133. Copyright 2017, Elsevier.

According to the classification of capacitive electrodes, SICs can be termed as pseudocapacitors because the anode material exhibits pseudocapacitive behavior.[103] In the case of pseudocapacitance, the charge storage mainly originates from the electron-transfer mechanism rather than the adsorption of ions, i.e., EDLC behavior.[104] Three different faradaic mechanisms are responsible for electrochemical capacitive features: underpotential deposition, redox pseudocapacitance and intercalation pseudocapacitance. In the case of underpotential

34

deposition, the ions are deposited on the metal-electrolyte interface when the potential is lower than the equilibrium potential for cation reduction.[103,105] As for redox pseudocapacitance, the charge storage occurs *via* redox reactions of adsorbed ions, which are accompanied by fast and reversible electron transfer across the electrode-electrolyte interface.[103,106] Lastly, the intercalation pseudocapacitance corresponds to the intercalation of active ions in a redox-active material without any phase transition.[107,108]

Recent studies suggest that some battery-type electrode materials with nanostructures might exhibit a faster charge/discharge rate compared to those without nanostructures, and capacitor-type electrode materials demonstrate improved capacitance with an increased outer surface area.[102-111] Therefore, several battery-type electrode materials showing faradaic behavior have been considered as pseudocapacitive electrodes,[112,113] which led to a fundamental confusion about pseudocapacitance. On the other hand, a number of studies reported that several electrode materials exhibit pseudocapacitive behavior during $Li^+/Na^+$ insertion, but the charge storage within the crystalline framework was not determined by the $Li^+$ or $Na^+$ diffusion process.[102,114-122] These devices are a combination of the typical faradaic behavior of battery-type electrodes and pseudocapacitive behavior of capacitor-type electrodes, causing further confusion and indicates that the pseudocapacitance

35

mechanism requires further investigation.

## 3.2 Classification of biomass-derived carbons

## 3.2.1 0D carbons

It has been reported that the carbonaceous materials with nanostructures are promising high-power faradaic electrodes for asymmetric supercapacitors.[123 - 127] The short ionic and electronic transport path gives rise to high power density, while the charge storage capacity is improved by the insertion of ions into graphitic crystallites. In addition, the carbon nanomaterials exhibit pseudocapacitive behavior, which further increases their power density.[128] Yun et al.[129] utilized silk fibroin as a carbon precursor to synthesize ultra-thin hollow carbon nanospheres (UTH-CNs) by using the hard-template method. The as-prepared UTH-CNs exhibited ultra-thin carbon walls (~3 nm), which are highly favoured for fast Na-ion transport and offer a large number of active sites. The electrochemical results revealed that UTH-CNs could deliver a reversible discharge capacity of 285 mAh g$^{-1}$, corresponding to a specific capacitance of 410 F g$^{-1}$ at a current density of 100 mA g$^{-1}$. Furthermore, UTH-CNs-based full batteries were constructed by using amorphous carbon as a cathode, which showed a specific capacitance of 186 F g$^{-1}$ at 100 mA g$^{-1}$, whilst a specific capacitance of 80 F g$^{-1}$ was maintained at 5 A g$^{-1}$.

### 3.2.2 1D carbons

A technological milestone was achieved by fabricating HICs by using nano-sized carbon as both the cathode and anode. In 2017, Song et al.[130] utilized bacterial cellulose as a carbon precursor to prepare a 3D porous anode structure with entangled carbon nanofibers (HP-CNWs, diameter: 10-20 nm) through direct carbonization. XPS characterization revealed the presence of oxygen and oxygen-/nitrogen-containing functional groups. It can be explained that the heteroatoms played a critical role in the formation of a thermostable conjugated structure below 300 ℃. Moreover, the surface functional groups remained attached to the carbon surface even after carbonization at 1200 ℃. The CV curves of HP-CNWs exhibited a linear increase in voltage between 0.1 and 1.5 V (*vs*. Na$^+$/Na), which indicated the pseudocapacitive Na-ion storage on topological defect sites of hexagonal carbon layers. Most of the reversible capacity was provided by pseudocapacitive Na-ion storage up to 1.5 V. Furthermore, surface-functionalized microporous carbon nanosheets (FM-CNSs) have been synthesized using waste coffee grounds. The SIC, consisting of HP-CNWs and FMCNS, exhibited a high energy density of 130.6 Wh kg$^{-1}$ at ~210 W kg$^{-1}$, a high power density of ~15260 W g$^{-1}$ at 43.6 Wh kg$^{-1}$ and stable performance over 3000 charge/discharge cycles.

### 3.2.3 2D carbons

2D porous carbons are particularly effective in enhacning the

electrochemical performance of SICs due to the efficient charge and mass transporation pathway.[69,131,132,133] Dong et al.[132] fabricated sheet-like porous carbon with a high N-doping level by using *k*-carrageenan as a precursor. During the synthesis process, the alkali metal nitrate plays tripe roles including template for the sheet-like morphology, activating agent and nitrogen resource. Specifically, the nitrate salt offers a high nitrogen content of 8.6-12.6 at.% for the framework. When this sheet-like porous carbon was employed as anode for SIBs, it provides a high reversible capacity of 419 mAh g$^{-1}$ at a current density of 50 mA g$^{-1}$. In addition, it acts as an anode for SIC and exhibits a high energy density of 110.8 Wh kg$^{-1}$ and 40.5 Wh kg$^{-1}$ respectively at 329 W kg$^{-1}$ and 12100 W kg$^{-1}$ as well as excellent cycle stability.

Carbonaceous materials with 2D morphology have also been used as a cathode for SICs. Chen et al.[133] used six different types of agricultural waste, including peanut shell, wheat straw, rice straw, corn stalk, cotton stalk, and soybean stalk, to fabricate carbonaceous materials that were then utilized as a positive electrode in Na-ion capacitors. These wastes-derived carbons presented a sheet-like morphology with a large number of micropores (< 2 nm) and mesopores (2-50 nm) as the cellulosic microfibrils were largely disconnected after hydrothermal treatment and chemical activation. The sheet-like morphology enables effective ionic diffusion and increased numbers of active sites for Na-ion

38

storage, resulting in improved charge storage capability. These biomass-derived carbons have been studied as a positive electrode in SICs, as shown in **Fig. 10b-d**. The operating voltage ranged from 2.0 and 4.2 V (*vs.* Na$^+$/Na) and the Na ions were stored *via* physical surface ion adsorption rather than bulk insertion. The cotton stalk-derived carbon exhibited the highest capacitance of 160.5 F g$^{-1}$ at 0.2 A g$^{-1}$, which decreased to 112.3 and 47.5 F g$^{-1}$ at the current density of 2 and 20 A g$^{-1}$, respectively. It can be concluded that when the morphology, porous structure, and electrical conductivity are similar, a higher specific surface area (or large pore volume) would result in better EDLC performance. The galvanostatic charge/discharge profiles of SIC, consisting of a cotton stalk-derived positive electrode and a $Na_2Ti_{2.97}Nb_{0.03}O_7$ negative electrode, exhibited a significantly different behavior from the charge/discharge curves of the as-prepared carbon in the voltage range of 0 V to 4.2 V. The difference originated from the charge storage behavior of the negative electrode, which exhibited intercalation-type Na-ion storage and resulted in non-linear charge/discharge curves. The Ragone plot shows that the energy density of SIC was 169.4 and 30.0 Wh kg$^{-1}$ at the power densities of 120.5 to 1865 W kg$^{-1}$, respectively. In addition, it is worth emphasizing that the studied SIC exhibited capacitance retention of 83.8 % after 500 cycles, demonstrating excellent potential for future development.

Carbon nanosheets serving as both the cathode and anode is a novel

39

way to reduce the cost for SICs. Wang et al.[69] synthesized carbon nanosheet from peanut skin, which exhibited a high performance as SIB anode, and also displayed excellent performance as SIC that constructed using their carbon nanosheets as both the cathode and anode. Specifically, the SIC presents energy density in the range of 112 to 45 Wh kg$^{-1}$ with the corresponding power density ranging from 67 to 12100 W kg$^{-1}$. Moreover, the SIC with the weight ratio of 1:2 and 1:4 displayed excellent cycling stability with a retention of 82% and 85% after 3000 cycles.

### 3.2.4 3D carbons

3D carbon frameworks possess an amorphous and disordered structure with a large number of interconnected channels, facilitating ionic migration.[134] Liu et al.[135] employed garlic as the carbon precursor to synthesize both anode and cathode electrodes for SICs using different approaches. The hard carbon based anode, prepared by simple pyrolysis, exhibited a block-like morphology with a smooth surface and irregular size. The as-prepared anode exhibited a high reversible capacity of 260 mAh g$^{-1}$ at 2 A g$^{-1}$, an ICE of 50.7% and capacity retention of 80% after 10000 charge/discharge cycles. On the cathode side, the porous carbon produced *via* the carbonization-activation process delivered a high capacity of 152 mAh g$^{-1}$ at 5 A g$^{-1}$ and capacity retention of 73% after 10000 charge/discharge cycles. Subsequently, the SIC, consisting of hard

carbon anode and porous carbon cathode, exhibited an excellent energy density of 156 Wh kg$^{-1}$ at a power density of 355 W kg$^{-1}$.

Recently, dual-carbon SICs have gained significant research interest, where cellulose-derived carbon was utilized as both the cathode and anode material.[136-138] The cellulose-derived carbon presented superior electrochemical performance, which can be ascribed to its unique morphology. It is noted that the carbonization of cellulose formed a 3D interconnected network, which provides a conductive carbon framework for efficient electron transport. The increased electrical conductivity enhanced electrode kinetics and reduced charge transfer resistance. It has been proposed that fast and efficient faradaic redox reactions occurred on the active surface area of the electrode.[138] The unique structure of cellulose-derived carbon strongly influenced the electrochemical performance of SICs. Specifically, the hierarchical micropore-mesopore structure increased the contact area between electrode and electrolyte, reduced the diffusion resistance and shortened the ionic diffusion distance. Moreover, the same carbon framework can be obtained by using a single carbon precursor. The porous structure resulted in a low charge transfer resistance and thus played a critical role in the charge/discharge process. Furthermore, the surface properties of cellulose-derived carbon also influenced the electrochemical performance of SICs. For instance, the functional groups presented in the cellulose-derived carbon materials

41

could provide extra active sites and/or moderate defects for sodium storage, thus improving surface pseudocapacitive charge storage.

## 3.3 Factors influence the performance for SICs

Similar to the prerequisites for SIBs, it is essential to optimize several inherent characteristics of biomass-derived carbons to achieve superior SIC performance. As mentioned earlier, carbonaceous materials with adjustable meso/microporous structures and high specific surface areas exhibit capacitor-like adsorption, whereas the higher degree of graphitic ordering endows battery-like ion intercalation behavior. Recently, several researchers studied biomass-derived carbons as both anode and cathode in SICs to overcome the problem of mismatch between both electrodes. In 2015, Mitlin et al.[131] reported a SIC with biomass-derived carbonaceous anode and cathode. Owing to the morphological differences between the inner and outer surfaces of the peanut shell, the smooth inner portion was employed as an anode and the rough outer section with a high specific surface area was employed as a cathode in SICs. Peanut shell nanosheet carbon (PSNC) exhibited a high specific surface area of 2396 $m^2$ $g^{-1}$ and high oxygen content of 13.51 wt.%, which led to a superior specific capacity of 161 mAh $g^{-1}$ and 73 mAh $g^{-1}$ at 0.1 A $g^{-1}$ and 25.6 A $g^{-1}$, respectively. Meanwhile, the peanut shell ordered carbon (PSOC) was utilized as an intercalation-type anode, which delivered a high specific capacity of 315 mAh $g^{-1}$ at 3.2 A $g^{-1}$.

42

Consequently, the assembled SIC, consisting of PSNC and PSOC, yielded energy densities of 201, 76 and 50 Wh kg$^{-1}$ at the power densities of 285, 8500 and 16500 W kg$^{-1}$, respectively. Moreover, the SIC retained 72% and 88% of the initial capacity after 10000 cycles at 6.4 A g$^{-1}$ and 100000 cycles at 51.2 A g$^{-1}$, respectively.

Furthermore, heteroatom doping can increase the active surface sites and defects for sodium storage. O- and N- co-doped carbons have been widely used as it provides additional charge-storage capacity by Na ions bond to the functional groups, and improves the electrical conductivity by introducing more free electrons to the conduction band of the carbon.[139-144] N-, S- and O-doped carbon can be facially synthesized due to the chemical diversity of natural resources. However, it is hard to control the content of dopants in biomass-derived carbon. Recently, Guo et al.[145] introduced an air oxidation activation (AOA) technique to finely tune the elemental composition of biomass-derived carbon. As shown in **Fig. 11a**, the anode material was further treated by the AOA technique, while the cathode material was prepared by carbonization/activation of cuttlebone. During the AOA process, the loss of the C atoms occurs at a faster rate than that for the N atoms, which increases the relative content of N-doping due to the fact that the C-N bond possesses higher binding energy than the C-C bond (**Fig. 11b**). On the other hand, the proportion of pseudocapacitance can be controlled by changing the air oxidation time.

Notably, the pseudocapacitance exhibits rapid Na ion storage kinetics, which is benficial for ultrafast charge/discharge capability and excellent cyclic performance. **Fig. 11c** presents a schematic illustration of the porosity evolution and an increase in pseudocapacitance of the carbon matrix with prolonged AOA treatment. The cuttlebone-derived carbonaceous sheets upon AOA-treatment for 2 h (CBCS-A3) exhibited an optimal combination of high specific surface area, hierarchical porosity and dopant (N and O) content, which contributed to the superior electrochemical performance. In addition, SIC was constructed by using the cuttlebone-derived carbon anode and cathode and its charge-storage mechanism is presented in **Fig. 11d**. Na ions were intercalated between the carbon layers or reacted with N and O in the anode, aided by the hierarchical porosity and high content of heteroatoms. On the other hand, $ClO_4^-$ ions were absorbed onto the surface of the porous cathode. The as-fabricated SIC delievered a high energy density of 95 Wh kg$^{-1}$ and 36 Wh kg$^{-1}$ at a power density of 1000 W kg$^{-1}$ and 53000 W kg$^{-1}$, respectively.
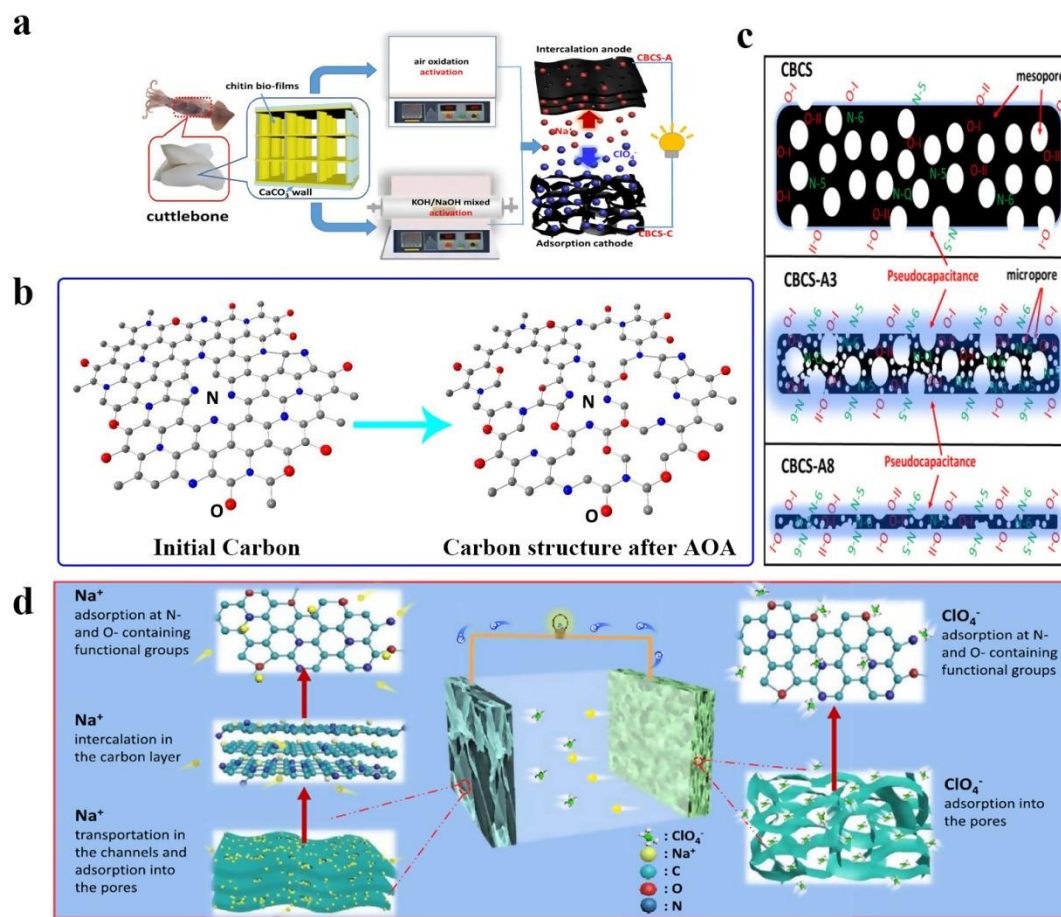
44

**Figure 11.** (a) Schematic illustration of the synthesis process and relevant anode/cathode charge-storage mechanisms in SICs; (b) schematic illustration of the structure of carbon materials with and without AOA treatment; (c) schematic illustration of the influence of AOA treatment time on porosity and pseudocapacitance of carbon matrix; and (d) schematic illustration of the charge-storage mechanisms of SICs. Reproduced (adapted) with permission from Ref. 145. Copyright 2018 American Chemical Society

## 4 Challenges for practical application

Despite the extraordinary progress made towards the biomass-based high-performance electrode for sodium storage (and also for other

electrochemical devices) recently, there is still one crucial yet less-explored aspect that restricts the practical application of these materials, i.e. the unstable supply of the raw material and thus inconsistence to the pyrolytic carbons, which is also credited to the nature. The inconsistence is generally related to the variation of the morphology caused by the growth condition of biomass, and also the composition of biomass, i.e. the inorganic residues and the diverse organic components.

There are numerous inorganic impurities exist in the biomass-derived carbon. These impurities usually are detriments and disadvantages for the self-discharge rate in SIB and SIC, although very few paper have discussed the purification and cleaning step so far.[146] Leaching combined rinsing is an effective purification method for removing the impurity in biomass-derived carbon [40,133,145- 153 ]. For examples, Li et al.[147] carefully washed graphene-like nanosheets by using 2 M hydrochloric acid (HCl) and distilled water to remove the remaining impurities. These carbonaceous materials provide a large reversible capacity and excellent rate performance as an anode for SIBs. Also, Niu et al.[154] use cattle bone as a precursor to synthesize hierarchically porous carbon nanosheets which was cleaned with 1 M HCl after carbonization. The SIC based on this hierarchically porous carbon nanosheets anode provided simultaneously high energy and power densities (105.2 Wh kg$^{-1}$ at 0.07 kW kg$^{-1}$, 32.5 Wh kg$^{-1}$ at an ultrahigh power density of 60.4

46

kW kg$^{-1}$), as well as good cyclic stability (85.8% of the capacitance retention after 4000 cycles at 3.5 A g$^{-1}$). Acid cleaning was operated before carbonization in some cases. For example, Wang et al. [152] use 6 M HCl and 10% HF to remove impurities in the rice husks before carbonization. Full SIBs assembled by using Na$_3$V$_2$(PO4)$_2$F$_3$/C and hard carbon derived from rice husks as cathode and anode respectively delivered a high-energy density of 185 Wh kg$^{-1}$. Furthermore, organic solutions have also been used to clean the biomass. Teng et al.[155] synthesized N-doped hard carbon miro-tubes (NCT) *via* carbonizing willow catkins after washing by acetone and water. The product showed a high reversible capacity, excellent rate performance and cyclic stability.

Nevertheless, the inorganic impurity also exerts positive effects to the carbonization process, which can optimize the microstructure and morphology, as well as improve the graphitization degree of the pyrolytic carbon [146, 156-159]. Ghimbeu et al.[146] reported that the presence of inorganic impurity such as sodium or potassium compounds contribute to the formation of pores during the pyrolysis resulting from an *in-situ* activation of the carbon. The pores increased the specific surface area significantly, and the open structure facilitated the electrolyte diffusion and enabled fast charge transfer and thus a larger reversible capacity. Furthermore, some impurity containing transition metal can serve as graphitization catalysts during carbonization. Hoekstra et al.[157] reported

47

that the iron nanoparticles catalyze the conversion of the amorphous carbon to graphitic carbon nanostructures. For SIBs and SICs, this change increases the conductivity and enhances the performance of carbonaceous material. Therefore, to utilize the catalytic effect of impurities and prevent its disadvantages, it might be sensible to remove the impurities after carbonization.

Possibly an even more challenging aspect is the large variation of organic composition (and thus morphology) in biomass of the same species but grown in different conditions. There are various organic components including the low oxygen ones such as lipids, lignin, the high-oxygen ones including hemicellulose and cellulose as well as the heteroatomic compounds like chitin and phycocolloids. These components possess different chemical structures and physical properties, and thus different carbonization behaviour. The inconsistence of the morphology and composition of the raw material severly hinder the practical application of the pyrolytic carbons. A scalable and more reproducible process converting various biomass into a high-performance carbonaceous materials should be developed. In a previous work, we first removed lignin from a fungus by hydrothermal treatment in KOH solution. The remaining polysaccharide was then carbonized sparately, which demonstrated a higher capacitance than that derived from the whole fungus. The performance improvement was attibuted to the more

48

uniform carbonization behavior of the undividual biopolymer than the crude fungus complex.[21] More recently, Feng et al.[160] proposed a process to produce high-performance hard carbon materials for SIBs *via* manipulating the component in different plant biomass. They removed non-lignocellulose (such as proteins, minerals, starch, etc) and hemicellulose from three type of biomass including Brewer's spent grain, grape pomace and walnut shells *via* chemical-enzymatic fractionation process in aicd solution to product acid detergent fibers (ADFs). The hard carbons derived from these ADFs all displayed excellent electrochemical properties. The simultaneous absence of non-lignocellulose and hemicellulose led to expanded (002) interlayer spacing which enhanced the specific capacity remarkably. This study provides a feasible method to prepare biomass-carbon with high consistence.

Bio-refinery, a concept of converting biomass into industrial commodity producets, might be another feasible method for transferring various biomass into carbonaceous materials with commercial viability.[161] Previous reports have already discussed the potential products such as biofuels, biochemicals, and bio-based materials synthesized from lignocellulosic biomass by thermochemical, biochemical and chemical processes.[162-165] Similarly, with some suitable biochemical technologies, biomass could also be transformed from low-cost biomass into various useful resources. It provides a guidance to

49

design effective convertion processes for the selective production of useful chemical which can be utilized for synthesizing high-preformance electrode materials for sodium storage.

## 5 Conclusion and outlook

With the rapid development of renewable energy sources, highly efficient and cost-effective energy storage systems are critically desired. Sodium-based energy storage systems, such as SIBs and SICs, are the most promising alternatives to the Li-based energy storage devices because of abundant sodium resources and comparable performance. Herein, we have reviewed the utilization of biomass-derived carbons as potential electrode materials for SIBs and SICs. We have described the principle and charge storage mechanism of carbonaceous material in SIBs and SICs and reviewed the published literature, focusing on understanding the Na storage phenomenon. Moreover, we have presented a detailed account of electrochemical performance and the property-performance relationship of biomass-derived carbons for SIBs and SICs.

Despite the great potential of biomass-derived carbon electrodes in SIBs and SICs, some problems need to be resolved before successful commercialization and widespread utilization. For instance, we need to develop a thorough understanding of the formation and role of a solid

50

electrolyte interface, which may lead to the development of rational electrode designs for advanced energy storage devices. Moreover, even though biomass-derived carbons have been extensively investigated as electrode materials in SIBs and SICs, the electrochemical performance is far below that of LIBs and LICs, which indicates that the novel strategies should be adopted to enhance the energy density and cyclic stability of Na-based energy storage devices. In addition, the practical utilization of biomass-derived carbon in full-cell SIBs and SICs requires careful charge and capacitance balancing of the positive and negative electrodes. Lastly, both academic and industrial communities should collaborate to demonstrate a practical sodium-based energy system by exploiting the potential of biomass-derived carbon.

## Acknowledgments

## References

1  J.Y. Hwang, S.T. Myung, Y.K. Sun, *Chem. Soc. Rev.* **2017**, 46, 3529-3614.

51

2  B. Dunn, H. Kamath, J.-M. Tarascon, *Science* **2011**, 334, 928-935.

3  Y. Nishi, *J. Power sources* **2001**, 100, 101-106.

4  N. Yabuuchi, K Kubota, M. Dahbi, S. Komaba, *Chem. Rev.* **2014**, 114, 11636-11682.

5  E. Llave, V. Borgel, K.J. Park, J.-Y. Hwang, Y.-K. Sun, P. Hartmann, F.-F. Chesneau, D. Aurbach, *ACS Appl. Mater. Interfaces* **2016**, 8, 1867-1875.

6  M.D. Slater, D. Kim, E. Lee, C.S. Johnson, *Adv. Funct. Mater.* **2013**, 23, 947-958.

7  T.B. Reddy, D. Linden, *Linden's Handbook of Batteries* McGraw-Hill, **2010**.

8  K. Mizushima, P.C. Jones, P.J. Wiseman, J.B. Goodenough, *Mater. Res. Bull.* **1980**, 15, 783-789.

9  A. S. Nagelberg, W. L. Worrell, *J. Solid State Chem.* **1979**, 29, 345-354.

10 J. P. Parant, R. Olazcuag, M. Devalett, C. Fouassie, *J. Solid State Chem.* **1971**, 3, 1-11.

11 C. Delmas, C. Fouassier, P. Hagenmuller, *Physica B+C* **1980**, 99, 81-85.

12 P. Adelhelm, P. Hartmann, C. L. Bender, M. Busche, C. Eufinger, J. Janek, *Beilstein J. Nano technol.* **2015**, 6, 1016-1055.

13 H.W. Wang, Y. Zhang, H.X. Ang, Y.Q. Zhang, H.T. Tan, Y.F. Zhang, Y.Y. Guo, J.B. Franklin, X.L. Wu, M. Srinivasan, H.J. Fan Q.Y. Yan, *Adv. Funct. Mater.* **2016**, 26, 3082-3093.

14 H.X. Li, J.W. Lang, S.L. Lei, J.T. Chen, K.J. Wang, L.Y. Liu, T.Y. Zhang, W.S. Liu, X.B. Yan, *Adv. Funct. Mater.* **2018**, 28, 1800757.

15 J.Y. Wan, F. Shen, W. Luo, L.H. Zhou, J.Q. Dai, X.G. Han, W.Z. Bao, Y. Xu, J. Panagiotopoulos, X.X. Fan, D. Urban, A, Nie, R. Shahbazian-Yassar, L.B. Hu, *Chem. Mater.* **2016**, 28, 6528- 6535.

52

16  M. Wang, Y. Yang, Z.Z. Yang, L. Gu, Q.W. Chen, Y. Yu, *Adv. Sci.* **2017**, 4, 1600468.

17  Y.M. Li, S.Y. Xu, X.Y. Wu, J.Z. Yu, Y.S. Wang, Y.S. Hu, H. Li , L.Q. Chen, X.J. Huang, *J. Mater. Chem. A* **2015**, 3, 71-77.

18  J. Wang, L. Yan, Q.J. Ren, L.L. Fan, F.M. Zhang, Z.Q. Shi, *Electrochim. Acta* **2018**, 291, 188-196.

19  P. Kalyani, A. Anitha, *Int. J. Hydrogen Energy* **2013**, 38, 4034-4045.

20  P. McKendry, *Bioresour. Technol.* **2002**, 83, 37-46.

21  L.B. Deng, W.H. Zhong, J.B. Wang, P.X. Zhang, H.M. Fang, L.Yao, X.Q. Liu, X.Z. Ren, Y.L. Li, *Electrochim. Acta* **2017**, 228, 398-406.

22  L. Yao, J.S. Lin, H.T. Yang, Q. Wu, D.R. Wang, X.J. Li, LB. Deng, Z.J. Zheng, *Nanoscale* **2019**, 11, 11086-11092.

23  W.J. Tang, Y.F. Zhang, Y. Zhong, T. Shen, X.L. Wang, X.H. Xia, J.P. Tu, *Mater. Res. Bull.* **2017**, 88, 234-241.

24  H. Jin, X.M. Wang, Z.R. Gu, J. Polin, *J. power sources* **2013**, 236, 285-292.

25  D.W. Zhang, G. Wang, L. Xu, J.B. Lian, J. Bao, Y. Zhao, J.X. Qiu, H.M. Li, *Appl. Surf. Sci.* **2018**, 451, 298-305.

26  E. M. Lotfabad, J. Ding, K. Cui, A. Kohandehghan, P. Kalisvaart, M. Hazelton, D. Mitlin, *ACS Nano* **2014**, 8, 7115-7129.

27  Y.H. Zheng, Y.S. Wang, Y.X. Lu, Y.-S. Hu, J. Li, *Nano Energy* **2017**, 39, 489-498.

28  L.B. Hu, H.Wu, F. La Mantia, Y.A. Yang, Y. Cui, *ACS Nano* **2010**, 4, 5843-5848.

29  P.R. Kumar, Y.H. Jung, S.A. Ahad, D.K. Kim, *RSC Adv.* **2017**, 7, 21820-21826.

30  F.J. García-Mateos, R. Berenguer, M.J. Valero-Romero, J.

Rodríguez-Mirasol, T. Cordero, *J. Mater. Chem. A* **2018**, 6, 1219-1233.

31  Y.M. Li, Y.-S. Hu, H. Li, L.Q. Chen, X.J. Huang, *J. Mater. Chem. A* **2016**, 4, 96-104.

32  W.L. Zhang, Y.J. Lei, F.W. Ming, Q. Jiang, Pedro M. F. J. Costa, H. N. Alshareef, *Adv. Energy Mater.* **2018**, 8, 1801840.

33  Q. Jiang, Z.H. Zhang, S.Y. Yin, Z.P. Guo, S.Q. Wang, C.Q. Feng, *Appl. Surf. Sci.* **2016**, 379, 73-82.

34  R.R. Gaddam, D.F. Yang, R. Narayan, KVSN Raju , N.A. Kumar, X.S. Zhao, *Nano Energy* **2016**, 26, 346-352.

35  F. Chen, J. Yang, T. Bai, B. Long, X.Y. Zhou, *J. Electroanal. Chem.* **2016**, 768, 18-26.

36  P. Sennu, V. Aravindan, M. Ganesan, Y.G. Lee, Y.S. Lee, *ChemSusChem* **2016**, 9, 849-854.

37  B. Li, F. Dai, Q.F. Xiao, L. Yang, J.M. Shen, C.M. Zhang, M. Cai, *Adv. Energy Mater.* **2016**, 6, 1600802.

38  H.B. Li, F. Shen, W. Luo, J.Q. Dai, X.G. Han, Y.N. Chen, Y.G. Yao, H.L. Zhu, K. Fu, E. Hitz, L.B. Hu, *ACS Appl. Mater. Interfaces* **2016**, 8, 2204-2210.

39  N. Zhang, Q. Liu, W.L. Chen, M. Wan, X.C. Li, L.L. Wang, L.H. Xue, W.X. Zhang, *J. Power Sources* **2018**, 378, 331-337.

40  Z.Y. Zhu, F. Liang, Z.R. Zhou, X.Y. Zeng, D. Wang, P. Dong, J.B. Zhao, S.G. Sun, Y.J. Zhang, X. Li, *J. Mater. Chem. A* **2018**, 6, 1513-1522.

41  M. Vadivazhagan, P. Parameswaran, U. Mani, K. Nallathamby, *ACS Sustainable Chem. Eng.* **2018**, 6, 13915-13923.

42  H. Chen, D. Liu, Z.H. Shen, B.F. Bao, S.Y. Zhao, L.M. Wu, *Electrochim. Acta* **2015**, 180, 241-251.

43  C.P. Ruan, K.L. Ai, L.H. Lu, *RSC Adv.* **2014**, 4, 30887-30895.

54

44  Z. Liu, Z. Zhu, J.D. Dai, Y.S. Yan, *ChemistrySelect* **2018**, 3, 5726-5732.

45  Y.P. Liu, Z.L. Li, L. Yao, S.M. Chen, P.X. Zhang, L.B. Deng, *Chem. Eng. J.* **2019**, 366, 550-559.

46  L.Yao, J.J. Yang, P.X. Zhang, L.B. Deng, *Bioresour. Technol.* **2018**, 256, 208-215.

47  J.Y. Kim, M.S. Choi, K.H. S, M. Kota, Y.B. Kang, S.J. Lee, J.Y. Lee, H.S. Park, *Adv. Mater.* **2019**, 31, 1803444.

48  Y.L. Cao, L.F. Xiao, M.L. Sushko, W. Wang, B. Schwenzer, J. Xiao Z.M. Nie, L.V. Saraf, Z.G. Yang, J. Liu, *Nano Lett.* **2012**, 12, 3783-3787.

49  W. Luo, Z.L. Jian, Z.Y. Xing, W. Wang, C. Bommier, M.M. Lerner, X.L. Ji, *ACS Cent. Sci.* **2015**, 1, 516-522.

50  S. Qiu, Y. Cao, X. Ai, H. Yang, *Sci Sin Chim*, **2017**, 47, 573-578.

51  D.A. Stevens, J.R. Dahn, *J. Electrochem. Soc.* **2001**, 148, A803-A811.

52  S. Qiu, L. Xiao, M.L. Sushko, K.S. Han, Y.Y. Shao, M.Y. Yan, X.M. Liang, L.Q. Mai, J.W. Feng, Y.L. Cao, X.P. Ai, H.X. Yang, J. Liu, *Adv. Energy Mater.* **2017**, 7, 1700403.

53  Y.M. Li, Y-S Hu, M-M Titirici, L.Q. Chen, X.J. Huang, *Adv. Energy Mater.* **2016**, 6, 1600659.

54  C. Bommier, T.W. Surta, M. Dolgos, X. Ji, *Nano Lett.* **2015**, 15, 5888 -5892.

55  N. Sun, Z. Guan, Y. Liu, Y. Cao, Q. Zhu, H. Liu, Z. Wang, P. Zhang, B. Xu, *Adv. Energy Mater.* 2019, 9, 1901351.

56  Q. Wang, H. Li, L.Q. Chen, X.J. Huang, *Carbon* **2001**, 39, 2211-2214.

57  B. Zhang, C.M. Ghimbeu, C. Laberty , C. Vix-Guterl, J. Tarascon, *Adv. Energy Mater.* **2016**, 6, 1501588.

55

58  Y. Huang, L. Wang, L. Lu, M.M. Fan, F.S. Yuan, B.J. Sun, J.S. Qian, Q.L. Hao, D.P. Sun, *New J. Chem.* **2018**, 42, 7407-7415.

59  A. Mirabedini, J. Foroughi, G.G. Wallace, *RSC Adv.* **2016**, 6, 44687-44716.

60  F.H. Yang, Z.A. Zhang, K. Du, X.X. Zhao, W. Chen, Y.Q. Lai, J. Li, *Carbon* **2015**, 91, 88-95.

61  X. Huang, X.Y. Qi, F. Boey, H. Zhang, *Chem. Soc. Rev.* **2012**, 41, 666-686.

62  L. Fu, K. Tang, K.P. Song, P.A. van Aken, Y. Yu, J. Maier, *Nanoscale* **2014**, 6, 1384-1389.

63  H.-G. Wang, Z. Wu, F.-L. Meng, D.-L. Ma, X.-L. Huang, L.-M. Wang, X.-B. Zhang, *ChemSusChem* **2013**, 6, 56-60.

64  J.H. Liu, X.W. Liu, *Adv. Mater.* **2012**, 24, 4097-4111.

65  T.Z. Yang, T. Qian, M.F. Wang, X.W. Shen, N. Xu, Z.Z. Sun, C.L. Yan, *Adv. Mater.* **2016**, 28, 539-545.

66  S. Komaba, W. Murata, T. Ishikawa, N. Yabuuchi, T. Ozeki, T. Nakayama, A. Ogata, K. Gotoh, K. Fujiwara, *Adv. Funct. Mater.* **2011**, 21, 3859-3867.

67  W. Luo, J. Schardt, C. Bommier, B. Wang, J. Razink, J. Simonsen, X.L. Ji, *J. Mater. Chem. A* **2013**, 1, 10662-10666.

68  Y.X. Wang, S.L. Chou, H.K. Liu, S.X. Dou, *Carbon* **2013**, 57, 202-208.

69  H. Wang, D. Mitlin, J. Ding, Z. Li, K. Cui, *J. Mater. Chem. A* 2016, 4, 5149-5158.

70  J.Y. Li, H. Qi, Q.G. Wang, Z.W. Xu, Y.J. Liu, Q.Y. Li, X.G. Kong, J.F. Huang, *Electrochim. Acta* **2018**, 271, 92-102.

71  P. Xue, N.N. Wang, Y.X. Wang, Y.H. Zhang, Y.L. Liu, B. Tang, Z.C. Bai, S.X. Dou, *Carbon* **2018**, 134, 222-231.

72  Y.Y. Zhu, M.M. Chen, Q. Li, C. Yuan, C.Y. Wang, *Carbon* **2018**,

129, 695-701.

73 P. liu, Y.M. Li, Y.S. Hu, H. L, L.Q. Chen, X.J. Huang, *J. Mater. Chem. A* **2016**, 4, 13046-13052.

74 P. Ruz, S. Banerjee, M. Pandey, V. Sudarsan, P.U. Sastry, R.J. Kshirsagar, *Solid State Sciences* **2016**, 62, 105-111.

75 H.S. Hou, X.Q. Qiu, W.F. Wei, Y. Zhang, X.B. Ji, *Adv. Energy Mater.* **2017**, 7, 1602898.

76 J. Ding, H.L. Wang, Z. Li, A. Kohandehghan, K. Cui, Z.W. Xu, B. Zahiri, X.H. Tan, E.M. Lotfabad, B.C. Olsen, D. Mitlin, *ACS Nano* **2013**, 7, 11004-11015.

77 J.S. Xia, N. Zhang, S.K. Chong, D. Li, Y. Chen, C.H. Sun, *Green Chem.* **2018**, 20, 694-700.

78 X.B. Jin, R. He, S. Dai, *Chem. Eur. J.* **2017**, 23, 11455-11459.

79 J.J. Peng, N.Q. Chen, R. He, Z.Y. Wang, S. Dai, X.B. Jin, *Angew. Chem.* **2017**, 129, 1777-1781.

80 L.F. Xiao, H.Y. Lu, Y.L. Fang, M. L. Sushko, Y.L. Cao, X.P. Ai, H.X. Yang, J. Liu , *Adv. Energy Mater.* **2018**, 8, 1703238.

81 X. Zhao, Y. Ding, Q. Xu, X. Yu, Y. Liu, H. Shen, *Adv. Energy Mater.* **2019**, 9, 1803648.

82 M.Z.A. Munshi. *Hand Book of Solid State Batteries & Capacitors*. World Scientific Publishing Co. pte. Ltd., Singapore, **1995**, P374.

83 T.Y. Zhang, L. Yang, X.B. Yan, X. Ding, *Small* **2018**, 14, 1802444.

84 A. Mahmood, S. Li, Z. Ali, H. Tabassum, B.J. Zhu, Z.B. Liang, W. Meng, W. Aftab, W.H. Guo, H. Zhang, M. Yousaf, S. Gao, R.Q. Zou, Y.S. Zhao, *Adv. Mater.* **2019**, 31, 1805430.

85 Y.-Y. Wang, B.-H. Hou, Q.-L. Ning, W.-L. Pang, X.-H. Rui, M.K. Liu, X.-L. Wu, *Nanotechnology* **2019**, 30, 214002.

86 M. Wahid, D. Puthusseri, Y. Gawli, N. Sharma, S. Ogale,

*ChemSusChem* **2018**, 11, 506-526.

87 Z.F. Li, C. Bommier, Z.S. Chong, Z.L. Jian, T.W. Surta, X.F. Wang, Z.Y. Xing, J.C. Neuefeind, W. F. Stickle, M. Dolgos, P.A. Greaney, X.L. Ji, *Adv. Energy Mater.* **2017**, 7, 1602894.

88 J.K. Ou, L. Yang, Z. Zhang, *J. Mater. Sci.: Mater. Electron* **2018**, 29, 16478-16485.

89 G. Wang, M. Shao, H.R. Ding, Y. Qi, J.B. Lian, S. Li, J.X. Qiu, H.M. Li, F.W. Huo, *Angew. Chem.* **2019**, 201908159.

90 H.W. Tao, M. Zhou, K.L. Wang, S.J. Chen, K. Jiang, *J. Alloys Compounds* **2018**, 754, 199-206.

91 P. Ge, H.S. Hou, S.J. Li, L. Yang, X.B. Ji, *Adv. Funct. Mater.* **2018**, 28, 1801765.

92 C.L. Yan, X. Gu, L. Zhang, Y. Wang, L.T. Yan, D.D. Liu, L.J. Li, P.C. Dai, X.B. Zhao, *J. Mater. Chem. A* **2018**, 6, 17371-17377.

93 Q.H. Wang, W.C. Zhang, C. Guo, Y.J. Liu, C. Wang, Z.P. Guo, *Adv. Funct. Mater.* **2017**, 27, 1703390.

94 D.H. Li, Y.Y. Sun, S. Chen, J.Y. Yao, Y.H. Zhang, Y.Z. Xia, D.J. Yang, *ACS Appl. Mater. Interfaces* **2018**, 10, 17175-17182.

95 B. Dursun, T. Sar, A. Ata, M. Morcrette, M.Y. Akbas, R. Demir-Cakan, *Cellulose* **2016**, 23, 2597-2607.

96 B.J. Yang, J.T. Chen, S.L. Lei, R.S. Guo, H.X. Li, S.Q. Shi, X.B. Yan, *Adv. Energy Mater.* **2018**, 8, 1702409.

97 R. Thangavel, K. Kaliyappan, K. Kang, X.L. Sun, Y.S. Lee, *Adv. Energy Mater.* **2016**, 6, 1502199.

98 Y.X. Wang, S.L. Chou, D. Wexler, H.K. Liu, S.X. Dou, *Chem. Eur. J.* **2014**, 20, 9607-9612.

99 S.H. Chen, J. Wang, L. Fan, R.F. Ma, E.J. Zhang, Q. Liu, B.A. Lu, *Adv. Energy Mater.* **2018**, 8, 1800140.

100 Z.Y. Le, F. Liu, P. Nie, X.R. Li, X.Y. Liu, Z.F. Bian, G. Chen,

58

H.B. Wu, Y.F. Lu, *ACS Nano* **2017**, 11, 2952-2960.

101 F. Li, Z. Zhou, *Small* **2018**, 14, 1702961.

102 Y.G. Wang, Y.F. Song, Y.Y. Xia, *Chem. Soc. Rev.* **2016**, 45, 5925-5950.

103 Y.L. Shao, M.F. El-Kady, J.Y. Sun, Y.G. Li, Q.H. Zhang, M.F. Zhu, H.Z. Wang, B Dunn, R.B. Kaner, *Chem. Rev.* **2018**, 118, 9233-9280.

104 J.S. Lin, L. Yao, Z.L. Li, P.X. Zhang, W.H. Zhong, Q.H. Yuan, L.B. Deng, *nanoscales* **2019**, 11, 3281-3291.

105 V. Sudha, M.V. Sangaranarayanan, *J. Phys. Chem. B* **2002**, 106, 2699-2707.

106 H.Y. Lee, J.B. Goodenough, *J. Solid State Chem.* **1999**, 144, 220-223.

107 L.P. Kong, C.F. Zhang, S.M. Zhang, J.T. Wang, R. Cai, C.X. Lv, W.M. Qiao, L.C. Ling, D.H. Long, *J. Mater. Chem. A* **2014**, 2, 17962-17970.

108 L.P. Kong, C.F. Zhang, J.T. Wang, W.M. Qiao, L.C. Ling, D.H. Long, *ACS Nano* **2015**, 9, 11200-11208.

109 N.S. Choi, Z.H. Chen, S.A. Freunberger, X.L. Ji, Y.K. Sun, K. Amine, G. Yushin, L.F. Nazar, J. Cho, P.G. Bruce, *Angew. Chem.* **2012**, 51, 9994-10024.

110 P. Simon, Y. Gogotsi, *Nat. Mater.* **2008**, 7, 845-854.

111 Q.F. Zhang, E. Uchaker, S.L. Candelaria, G.Z. Cuo, *Chem. Soc. Rev.* **2013**, 42, 3127-3171.

112 S.G. Kandalkar, J.L. Gunjakar, C.D. Lokhande, *Appl. Surf. Sci.* **2008**, 254, 5540-5544.

113 B. Senthilkumar, R.K. Selvan, L. Vasylechko, M. Minakshi, *Solid Stated Sci.* **2014**, 35, 18-27.

114 M. Zukalová, M. Kalbáč, L. Kavan, Ivan Exnar, M. Graetzel, *Chem.*

Accepted Manuscript

59

*Mater.* **2005**, 17, 1248-1255.

115 J.R. Li, Z.L. Tang, Z.T. Zhang, *Chem. Phys. Lett.* **2006**, 418, 506-510.

116 J. Wang, J. Polleux, J. Lim, B. Dunn, *J. Phys. Chem. C* **2007**, 111, 14925-14931.

117 Y.G. Wang, Z.S. Hong, M.D. Wei, Y.Y. Xia, *Adv. Funct. Mater.* **2012**, 22, 5185-5193.

118 K. Brezesinski, J. Wang, J. Haetge, C. Reitz, S.O. Steinmueller, S.H. Tolbert, B.M. Smarsly, B. Dunn, T. Brezesinski, *J. Am. Chem. Soc.* **2010**, 132, 6982-6990.

119 T. Brezesinski, J. Wang, S.H. Tolbert, B. Dunn, *Nat. Mater.* **2010**, 9, 146-151.

120 V. Augustyn, J. Come, M.A. Lowe, J.W. Kim, P.L. Taberna, S.H. Tolbert, H.D. Abruña, P. Simon, Bruce Dunn, *Nat. Mater.* **2013**, 12, 518-522.

121 M. Sathiya, A.S. Prakash, K. Ramesha, J.-M. Tarascon, A.K. Shukla, *J. Am. Chem. Soc.* **2011**, 133, 16291-16299.

122 V. Augustyn, P. Simon, B. Dunn, *Energy Environ. Sci.* **2014**, 7, 1597-1614.

123 L. Qie, W.M. Chen, Z. H. Wang, Q.G. Shao, X. Li, L.X. Yuan, X.L. Hu, W.X. Zhang, Y.H. Huang, *Adv. Mater.* **2012**, 24, 2047-2050.

124 B.Z. Jang, C.G. Liu, D. Neff, Z.N. Yu, M.C. Wang, W. Xiong, A. Zhamu, *Nano Lett.* **2011**, 11, 3785-3791.

125 Z.J. Fan, Y. Liu, J. Yan, G.Q. Ning, Q. Wang, T. Wei, L.J. Zhi, F. Wei, *Adv. Energy Mater.* **2012**, 2, 419-424.

126 H. Zhang, G.P. Cao, Y.S. Yang, *Energy Environ. Sci.* **2009**, 2, 932-943.

127 S.B. Yang, X.L. Feng, L.J. Zhi, Q. Cao, J. Maier, K. Müllen, *Adv. Mater.* **2010**, 22, 838-842.

128  P. Simon, Y. Gogotsi, B. Dunn, *Science* **2014**, 343, 1210-1211.

129  Y.S. Yun, S.Y. Cho, H. Kim, H.J. Jin, K. Kang, *ChemElectroChem* **2015**, 2, 359-365.

130  M.Y. Song, N.R. Kim, S.Y. Cho, H.-J. Jin, Y.S. Yun, *ACS Sustainable Chem. Eng.* **2017**, 5, 616-624.

131  J. Ding, H.L. Wang, Z. Li, K. Cui, D. Karpuzov, X.H. Tan, A. Kohandehghan, D. Mitlin, *Energy Environ. Sci.* **2015**, 8, 941-955.

132  G.H. Dong, H.L. Wang, W. Liu, J. Shi, S.J. Sun, D. Li, H. Zhang, Y.P. Yang, Y.P. Cui, *ACS Appl. Energy Mater.* **2018**, 1, 5636-5643.

133  J.Z. Chen, X.Y. Zhou, C.T. Mei, J.L. Xu, S. Zhou, C.P. Wong, *J. Power Sources* **2017**, 342, 48-55.

134  P.Y. Wang, B.J. Yang, G.H. Zhang, L. Zhang, H.Y. Jiao, J.T. Chen, X.B. Yan, *Chem. Eng. J.* **2018**, 353, 453-459.

135  H.L. Liu, X. Liu, H.L. Wang, Y.L. Zheng, H. Zhang, J. Shi, W. Liu, M.H. Huang, J.L. Kan, X.C. Zhao, D. Li, *ACS Sustainable Chem. Eng.* **2019**, 7, 12188-12199.

136  W.S. Chen, H.P. Yu, S.Y. Lee, T. Wei, J. Li, Z.J. Fan, *Chem. Soc. Rev.* **2018**, 47, 2837-2872.

137  M.Y. Song, N.R. Kim, S.Y. Cho, H.-J. Jin, Y.S. Yun, *ACS Sustainable Chem. Eng.* **2017**, 5, 616-624.

138  Q.Y. Xia, H. Yang, M. Wang, M. Yang, Q.B. Guo, L.M. Wan, H. Xia, Y. Yu, *Adv. Energy Mater.* **2017**, 7, 1701336.

139  W.H. Yu, H.L. Wang, S. Liu, N. Mao, X. Liu, J. Shi, W. Liu, S.G. Chen, X. Wang, *J. Mater. Chem. A* **2016**, 4, 5973-5983.

140  Y.M. Li, Z.G. Wang, L.L. Li, S.J. Peng, L. Zhang, M. Srinivasan, S. Ramakrishna, *Carbon* **2016**, 99, 556-563.

141  H.G. Wang, Z. Wu, F.L. Meng, D.L. Ma, X.L. Huang, L.M. Wang, X.B. Zhang, *ChemSusChem* **2013**, 6, 56-60.

142  Y. Qiao, M.Y. Ma, Y. Liu, S. Li, Z.S. Lu, H.Y. Yue, H.Y. Dong,

61

Z.X. Cao, Y.H. Yin, S.T. Yang, *J. Mater. Chem. A* **2016**, 4, 15565-15574.

143 X.P. Wang, L.X. Lv, Z.H. Cheng, J. Gao, L.Y. Dong, C.G. Hu, C.G. Hu, L.T. Qu, *Adv. Energy Mater.* **2016**, 6, 1502100.

144 Y.W. Zhu, S. Murali, M.D. Stoller, K.J. Ganesh, W.W. Cai, P.J. Ferreira, A Pirkle, R.M. Wallace, K.A. Cychosz, M. Thommes, D. Su, E.A. Stach, R.S. Ruoff, *Science* **2011**, 332, 1537-1541.

145 Y.Q. Guo, W. Liu, R.T. Wu, L.J. Sun, Y. Zhang, Y.P. Cui, S. Liu, H.L. Wang, B.H. Shan, *ACS Appl. Mater. Interfaces* **2018**, 10, 38376-38386.

146 C.M. Ghimbeu, B. Zhang, A.M. de Yuso, B. Réty, J.-M. Tarascon, *Carbon* **2019**, 153, 634-647.

147 J.Y. Li, H. Qi, Q.G. Wang, Z.W. Xu, Y.J. Liu, Q.Y. Li, X.G. Kong, J.F. Huang, *Electrochim. Acta* **2018**, 271, 92-102.

148 D.W. Zhang, G. Wang, L. Xu, J.B. Lian, J. Bao, Y. Zhao, J.X. Qiu, H.M. Li, *Appl. Surf. Sci.* **2018**, 451, 298-305.

149 N. Zhang, Q. Liu, W.L. Chen, M. Wan, X.C. Li, L.L. Wang, L.H. Xue, W.X. Zhang, *J. Power Sources* **2018**, 378, 331-337.

150 Q. Jiang, Z.H. Zhang, S.Y. Yin, Z.P. Guo, S.Q. Wang, C.Q. Feng, *Appl. Surf. Sci.* **2016**, 379, 73-82.

151 J.K. Ou, L. Yang, X.H. Xi, *Electron. Mater. Lett.* **2017**, 13, 66-71.

152 Q.Q. Wang, X.S. Zhu, Y.H. Liu, Y.Y. Fang, X.S. Zhou, J.H. Bao, *Carbon* **2018**, 127, 658-666.

153 E.C. Hao, W. liu, S. Liu, Y. Zhang, H.L. Wang, S.G. Chen, F.L.

Cheng, S.P. Zhao, H.Z. Yang, *J. Mater. Chem. A*, **2017**, 5, 2204-2214.

154  J. Niu, J.J. Liang, R. Shao, M.Y. Liu, M.L. Dou, Z.L. Li, Y.Q. Huang, F. Wang, *Nano Energy* **2017**, 41, 285-292.

155  Y.Q. Teng, M.S. Mo, Y. Li, *J. Electrochem. En. Conv. Stor.* **2018**, 15, 041010.

156  A. Oya, S. Otani, *Carbon* **1979**, 17, 131-137.

157  J. Hoekstra, A.M. Beale, F. Soulimani, M. Versluijs-Helder, D. Van De Kleut, J.M. Koelewijn, J.W. Geus, L.W. Jenneskens, *Carbon* **2016**, 107, 248-260.

158  C. Xia, S.Q. Shi, *Green Chem.* **2016**, 18, 2063-2071.

159  Y. Li, Z. Teng, P. Chen, Y. Song, Y. Luo, Q. Wang, *J. Colloid Interface Sci.* **2015**, 438, 130-137.

160  Y. Feng, L. Tao, Y. He, Q. Jin, C. Kuai, Y. Zheng, M. Li, Q. Hou, Z. Zheng, F. Lin, H. Huang, Chemical-enzymatic fractionation to unlock the potential of biomass-derived carbon materials for sodium ion batteries, *J. Mater. Chem. A* **2019**, 7, 26954-26965.

161  A. Bayu, A. Abudula, G. Guan, *Fuel Processing Technology* **2019**, 196, 106162.

162  C. Huang, H.-J. Guo, H.-R. Zhang, L. Xiong, H.-L. Li, X.-D. Chen, *J. Chem. Technol. Biotechnol.* **2019**, 94, 2416-2424.

163  F. Cherubini, *Energy Convers. Manage* **2010**, 51, 1412-1421.

63

164  V. Menon, M. Rao, *Prog Energy Combust Sci.* **2012**, 38, 522-550.

165  G. Taylor, *Energy Policy* **2008**, 36, 4406-4409.